



www.sciencemag.org/cgi/content/full/science.aaf1328/DC1

Supplementary Materials for

SCS macrophages suppress melanoma by restricting tumor-derived vesicle–B cell interactions

Ferdinando Pucci, Christopher Garris, Charles P. Lai, Andita Newton,
Christina Pfirschke, Camilla Engblom, David Alvarez, Melissa Sprachman,
Charles Evavold, Angela Magnuson, Ulrich H. von Andrian, Katharina Glatz,
Xandra O. Breakefield, Thorsten R. Mempel, Ralph Weissleder, Mikael J. Pittet*

*Corresponding author. E-mail: mpittet@mgh.harvard.edu

Published 17 March 2016 on *Science* First Release
DOI: 10.1126/science.aaf1328

This PDF file includes:

Materials and Methods

Figs. S1 to S27

Table S1

References

Materials and Methods

Generation of B16F10 tumors expressing tEV markers

We used lentiviral vectors that code for secreted and membrane-bound Gaussia Luciferase (sGLuc and mGLuc, respectively) as previously described (10). A lentiviral transfer plasmid that codes for CD63-eGFP and dLNGFR was cloned from an eGFP-dLNGFR bidirectional plasmid (30) and from a commercial CD63 coding plasmid (System Biosciences Inc.). We used dLNGFR for flow cytometry analyses and CD63-GFP for imaging experiments. dLNGFR staining is brighter than CD63-GFP staining by flow cytometry. However, because the commercial mouse anti-human CD271 Ab, which detects dLNGFR, can yield non-specific immunofluorescence staining in murine samples, we used CD63-GFP for imaging experiments. A lentiviral transfer plasmid that codes for CRE (without NLS, nuclear localization signal) and dLNGFR was cloned from the above bidirectional plasmid and synthetic CRE sequence was inserted (Integrated DNA Technologies). Lentiviral transfer plasmids coding for Rab35^{WT} and Rab35^{S22N} were generated by subcloning from plasmids #47424 and #47426, respectively (Addgene). Lentiviral vectors for H2B-Apple were kindly provided by Dr. Katherin S. Yang (Weissleder lab). B16F10 cells (ATCC) were plated at a concentration of 10⁵ cells per well in a 6-well plate and transduced with non-concentrated lentiviral vector supernatants (1:1 ratio with IMDM containing heat-inactivated FBS) in the presence of 1 µg/ml polybrene (Millipore). To generate cells carrying 1 copy of lentivector per genome (e.g. Rab35 experiments), 10-fold diluted lentivectors were titered on the cells plated as described above. Dilution that produced less than 20% transduced (i.e. dLNGFR⁺) cells (measured 1 week after transduction, to avoid pseudo-transduction) was flow sorted for purity. Non-concentrated VSV.G-pseudotyped, third-generation lentiviral stocks were produced and titered as described previously (31).

tEV purification

B16F10 cell supernatants were collected at >70% confluence and centrifuged at 2,000 g to remove non-adherent cells. The resulting supernatants were placed into ultracentrifugation tubes (Beckman), with ~5 ml left above the pellet (containing dead cells and large cell debris), and ultracentrifuged at 100,000 g for 1 h to pellet tEVs. After quickly pouring out the supernatants and blotting the tubes upside down on a paper towel, the tEV pellets were resuspended in 50 µl of PBS per ultracentrifugation tube and stored at -80°C. tEV preparations were quantified using the Bradford assay and the resulting protein contents ranged between 800 and 1,200 µg/ml. PKH67 labeling of tEVs (to validate our genetic marking approach *in vitro* and for tEV pulldown experiments) was performed following standard PKH67 labeling specifications and involved washing excess dye by ultracentrifugation as above.

Transmission electron microscopy of tEVs

A negative staining procedure for transmission electron microscopy was performed by floating Formvar/carbon coated grids (glow discharged) on a 5 µl drop of the sample on parafilm for 1 min. The grid was then moved to a drop of double-distilled water and excess liquid was removed with filter paper. Staining was performed by floating the grid on a small drop of 0.75% uranyl formate for 30 seconds. After removing the excess uranyl formate with filter paper, the grid was examined in a JEOL 1200EX Transmission electron microscope and images were recorded with an AMT 2k CCD camera at a primary magnification of 20,000-50,000x.

Mice and tumor challenge

Six to eight week old C57BL/6 mice and *Rosa26-Loxp-STOP-Loxp-eYFP* mice were purchased from Jackson Labs. *Cd169^{Dir}* transgenic mice (*Siglec1^{tm1(HBEGF)Mtk}*) were

kindly provided by the Riken Institute (Japan). Mice were assigned to experiments one week after arrival and all procedures were performed after approval from the Institutional Animal Care and Use Committee at MGH. For tumor challenge, B16F10 or B16F1 cells (ATCC) were injected either subcutaneously ($5 \cdot 10^5$ in 100 μ l of PBS) or intradermally ($1 \cdot 10^5$ in 50 μ l of HBSS) in the flank. KP1.9 lung adenocarcinoma cells (kindly gifted by Dr. Alfred Zippelius, University Hospital Basel, Switzerland) were injected intradermally ($2.5 \cdot 10^5$ in 50 μ l of HBSS) in the flank. The KP1.9 cell line derives from lung adenocarcinomas of C57BL/6 *Kras*^{LSL-G12D/+}; *p53*^{fl/fl} mice (referred to as KP (32)). Tumor volumes were calculated after caliper measurements of two axes using the formula: (width²•length)/2 where width<length. Tumor volumes from d 11 are shown unless otherwise specified.

Bioluminescence studies

mGLuc⁺ and mGLuc⁻ tEVs were placed in 96-well plates. Immediately after 1 μ g of coelenterazine (Prolume) was added, the samples were imaged with a Xenogen IVIS Imaging System 100. Organs and biofluids from mice carrying mGLuc⁺ B16F10 tumors were lysed and their bioluminescence activity was measured as described (10). To obtain bioluminescence images of whole tissues, mice carrying mGLuc⁺ B16F10 tumors were injected intravenously with 75 μ g of coelenterazine (Prolume) and euthanized 1 min later to image surgically explanted tissues. The amount of time between substrate injection and bioluminescence imaging was < 2 min.

Flow cytometry-based tEV detection

To detect tEVs by flow cytometry, we first prepared a cytometer (LSRII) to eliminate nano-sized physical contaminants. To this end, the air filter was removed while first 2 liters of warm 20% bleach and then 2 liters of warm distilled water (Millipore) were flushed through the system. After replacing the tank sheath fluid and putting the air filter back in place, 4 ml of 10% contrad (Fisher) was put in a facs tube and allowed to flow through the system. This procedure was then repeated with 4 ml of Windex, then with 4 ml of distilled water. Priming was performed after running each solution. The entire preparatory procedure takes ~4 h and ensures that electronic noise is the only signal detectable at the lowest possible threshold (200 on an LSRII). Size-standard nanoparticles (40 nm and 1000 nm, measured with a Malvern Instrument) were kindly provided by Dr. Nikolay Sergeev. Microbeads (7.5 μ m) were from Miltenyi. Membrane labeling with PKH67 (Sigma) was performed according to vendor instructions. For labeling tEV surface markers, fluorochrome-conjugated Abs were added to tEV preparations, which were subsequently analyzed without washing. Controls containing only fluorochrome-conjugated Abs were used to test for the presence of fluorochrome-containing aggregates the size of tEVs. Abs used are CD9, CD81 and anti-human CD271 (dLNGFR), all from Biolegend. CD63-eGFP was detected by direct fluorescence.

Cell tracking by photoconversion

Photoconversion experiments were performed using C57BL/6 Kaede mice (kindly provided by the Mathis lab) as previously described (12). Briefly, tumor-bearing mice were anesthetized with isoflurane. Overlying fur was already removed at the time of tumor injection. Mice were placed on their tumor-free flank and tape was applied over the inguinal area to protect the inguinal LN from UV light. A UV laser (Electra Pro Series Violet Handheld Laser; Laserglow Technologies) was shone (405 nm; peak power <5 mW; sustained power: 0.5–4.9 mW) onto the exposed area for 5 min. To ensure the whole tumor mass was exposed to UV light, a lens was attached to the laser to defocus the light beam. The source of the defocused light beam was positioned ~18 cm above the mouse;

the light beam diameter was ~1 cm. Flow cytometry-based detection of photoconverted cells was performed with a 561 nm laser.

Lymph collection

Thoracic duct cannulation was performed as described (33). Briefly, mice were given olive oil orally ~45 min prior to surgery to help visualize the lymphatic vessel network and the cisterna chyli. Mice were anesthetized by intraperitoneal injection of 100 mg/kg Ketamine HCl, 10 mg/kg Xylazine and 3 mg/kg Acepromazine. Mice then received a sterile heparinized polyethylene catheter in the right jugular vein for continuous fluid administration (1 U/ml Heparin in Ringer's lactate) throughout the procedure. Next, the thoracic duct and cisterna chyli were exposed by blunt dissection along the left posterior wall of the abdominal aorta between the diaphragm and renal vessels. A sterile cannula was carefully inserted into the thoracic duct and secured by tissue glue, with the remaining tubing exteriorized through the posterior abdominal wall. Approximately 100-500 μ l of lymph fluid was collected into sterile eppendorf tubes. Lymph cells were pelleted by centrifugation at 300 g.

Human samples

Paraffin-embedded sentinel LN tissue from 13 melanoma patients was obtained from the Institute for Pathology, Basel, Switzerland (from years 2005-2014). All sentinel nodes were cut along their longitudinal axis in 2 mm thick slices and embedded in their entirety in paraffin blocks. Four sequential 5 μ m-thick tissue sections were cut from each block and stained with hematoxylin and eosin (on sections 1 and 4) and immunohistochemically for HMB-45 (on sections 2 and 4; Ventana, anti-Melanosome, Clone: HMB-45, Dilution: RTU). Metastases had been excluded by microscopic examination of all LNs used for this study. The LNs were then microscopically evaluated for the presence of HMB-45-positive cells with macrophage morphology. The presence of HMB-45-positive macrophages was confirmed immunohistochemically by additional CD68 staining (CD68 DAKO/FLEX, Clone: PG-M1, Dilution: RTU). Secondary detection reagents included: Basic AEC Detection Kit, Ventana Medical Systems, orange-brown reaction product, Fig 2C (top panels). UltraView Red Detection Kit, Ventana Medical Systems, bright red reaction product, Fig 2A, Fig 2B, Fig 2C (bottom panel), Fig S13 (central panel). UltraView DAB Detection Kit Ventana Medical Systems, brown reaction product, Fig S13 (right panel).

In vivo LN cell transduction

Concentrated, VSV-pseudotyped, Cre-expressing lentiviral vectors were generated and titered as previously described (31) and injected i.d. (10^8 TU in 50 μ l) in *Rosa26-Loxp-STOP-Loxp-eYFP* mice. LNs draining the injection site were collected 5 days after injection.

Depletion of LN macrophages

To deplete inguinal LN SCS macrophages in C57BL/6 mice without affecting other phagocytes in the tumor bed, clodronate-loaded liposomes (Clo-Lip) (clodronateliposomes.org) were injected s.c. in the calf (50 μ l) 6 days before tumors were implanted in the flank. PBS-loaded liposomes (PBS-Lip) were used as controls. The liposome solution drains to the LN in less than 30 min, leaving the site of injection unaffected. To deplete SCS macrophages in *Cd169^{Dtr/Wt}* mice, diphtheria toxin (DT) was injected intraperitoneally (500 ng in 100 μ l) or s.c. (250 ng in 50 μ l) 2 d before tumor challenge. Either wild-type mice receiving DT or *Cd169^{Dtr/Wt}* mice that did not receive DT were used as controls. CD169-expressing macrophages were systemically depleted by intraperitoneal injection, whereas popliteal and inguinal LN macrophages were

ipsilaterally depleted by s.c. injection in the calf. Ipsilateral depletion was incomplete after injecting 50 ng of DT in the foot (data not shown). SCS macrophage depletion efficacy, triggered using the above approaches, was verified by imaging and flow cytometry.

BLZ945 treatment

The CSF1R inhibitor BLZ945 was synthesized as previously described (34) and formulated in 20% Captisol (Trappsol, USP grade) at concentrations in the range of 16.5-19 mg/ml. To ensure complete dissolution, the formulation was centrifuged. If no precipitate was observed, the concentration was based on the mass of BLZ945 and volume of Captisol solution. If a precipitate was observed, the supernatant was transferred to fresh tubes. BLZ945 concentration was determined using LCMS (comparison to a standard curve generated using DMF or DMSO solutions of BLZ945). For *in vivo* dosing, mice received 200 mg per kg body weight of BLZ945 or vehicle (20% Captisol) by intraperitoneal injection once daily for 5 days.

Flow cytometry

Tumors, spleens and bone marrow were mechanically dissociated into single cell suspensions. Lungs and inguinal LNs were made into single cell suspensions by enzymatic treatment as described (35). Cell suspensions were then stained with directly conjugated Abs (Biolegend, BD or eBiosciences) and 7AAD (Sigma). We labeled tumor cells and tEVs with dLNGFR because it is present only on tEVs and not on host cell EVs. In all experiments, cells of interest were identified as follows:

Lymph nodes

- Lymphoid cells (7AAD⁻ CD3⁺ or B220⁺ CD11b⁻ CD11c⁻);
- Myeloid cells (7AAD⁻ CD3⁻ B220⁻ CD11b⁺ or CD11c⁺);
- Medullary sinus macrophages (7AAD⁻ CD3⁻ B220⁻ CD11b⁺⁺ CD11c^{LO} CD169⁺ F4/80⁺ SSC^{HI});
- Medullary cord macrophages (7AAD⁻ CD3⁻ B220⁻ CD11b⁺⁺ CD11c^{LO} CD169⁻ F4/80⁺);
- Subcapsular sinus macrophages (7AAD⁻ CD3⁻ B220⁻ CD11b⁺ CD11c^{LO}CD169⁺F4/80⁻SSC^{LO});
- Dendritic cells (7AAD⁻ CD3⁻ B220⁻ CD11c^{HI});
- Others (7AAD⁻ CD3⁻ B220⁻ CD11b⁻ CD11c⁻);
- B cells (7AAD⁻ CD11b⁻ CD3⁻ B220⁺);
- CD8 T cells (7AAD⁻ CD11b⁻ B220⁻ CD4⁻ CD8⁺);
- CD4 T cells (7AAD⁻ CD11b⁻ B220⁻ CD4⁺ CD8⁺);
- Plasma cells (7AAD⁻ CD3⁻ CD19⁻ CD138⁺);
- Tumor cells (7AAD⁻ CD45⁻ dLNGFR⁺⁺⁺ CD31⁻);
- Non-hemopoietic (7AAD⁻ CD45⁻).

Skin

- Macrophages (7AAD⁻ CD45⁺ CD11b⁺ Ly6G⁻ F4/80⁺);
- Neutrophils (7AAD⁻ CD45⁺ CD11b⁺ Ly6G⁺ F4/80⁻);
- Dendritic cells (7AAD⁻ CD45⁺ CD11c⁺ Ly6G⁻ F4/80⁻).

Tumor

- Tumor cells (7AAD⁻ CD45⁻ dLNGFR⁺⁺⁺);
- Macrophages (7AAD⁻ CD45⁺ CD11b⁺ Ly6G⁻);
- Monocytes (7AAD⁻ CD45⁺ CD11b⁺ CD115⁺);
- Neutrophils (7AAD⁻ CD45⁺ CD11b⁺ Ly6G⁺);

- Dendritic cells (7AAD– CD45+ CD11c+ F4/80–);
- B cells (7AAD– CD45+ CD11b– CD19+);
- CD8 T cells (7AAD– CD45+ CD11b– CD8+);
- CD4 T cells (7AAD– CD45+ CD11b– CD4+);
- Endothelial cells (7AAD– CD45– CD31+);
- Myeloid cells (7AAD– CD45+ CD11b+);
- NK cells (7AAD– CD45+ NK1.1+ CD49b+);
- NKT cells (7AAD– CD45+ NK1.1+ CD49b+ CD3+);
- ILC (7AAD– CD19– CD4– CD8– gdTCR– NK1.1– CD49b– CD11b– CD90+ CD3–).

Bone marrow

- Neutrophils (7AAD– CD45+ CD11b+ CD117– CD115– SiglecF–);
- Eosinophils (7AAD– CD45+ CD11b+ CD117– CD115– SiglecF+);
- Monocytes (7AAD– CD45+ CD11b+ CD117– CD115+ SiglecF–);
- Macrophages (7AAD– CD45+ CD11b+ CD117– CD115– SiglecF– F4/80+);
- MDP (7AAD– CD45+ CD117+ Sca1– CD115+);
- HPC (7AAD– CD45+ CD117+ Sca1–);
- HSC (7AAD– CD45+ CD117+ Sca1+);
- DC (7AAD– CD11c+ CD3– CD19–);
- B cells (7AAD– CD11b– CD115– CD3– CD19+);
- T cells (7AAD– CD11b– CD115– CD3+ CD19–);
- Others (7AAD– CD11b– CD115– CD3– CD19– CD117–).

Spleen

- Monocytes (7AAD– CD45+ CD11b+ CD115+);
- Marginal zone macrophages (7AAD– CD45+ CD11b+ CD169+).

Eleven-color analyses were performed on a custom LSRII (BD) equipped with:

- 405nm laser and, in order, 450/50, 505LP, 515/20, 600LP, 610/20, 685LP, 695/40 filters;
- 488nm laser and, in order, 488/10, 505LP, 530/30, 550LP, 575/26, 685LP, 695/40 filters;
- 633nm laser and, in order, 660/20, 710LP, 730/45, 735LP, 780/60.

Fluorochromes employed were, in order: BV421 or eFluor450, BV510, BV605, BV711, FITC or eGFP or eYFP, PE, 7AAD or PerCP-Cy5.5, PE-Cy7, APC, Alexa700, APC-Cy7 or APC-eFluor780.

Imaging flow cytometry

Tumors were mechanically dissociated into single-cell suspensions. Cell suspensions were stained with directly-conjugated Abs (Biolegend) and 7AAD (Sigma) to identify tumor-associated cells (7AAD– CD45+ CD11b+) containing spotted fluorescence for CD63-eGFP or dLNGFR. The samples were analyzed on an Amnis ImageStreamX mkII Imaging Flow Cytometer with 405nm, 488nm, 642nm lasers and dual camera, at 20x magnification.

Detection of cytokines and chemokines in cell culture supernatants

To investigate the cytokine and chemokine profile in cell culture supernatants of B16F10 tumor cell lines carrying one copy of either Rab35-WT LV or Rab35-S22N LV, a membrane-based sandwich immunoassay was performed using the Proteome Profiler Mouse Cytokine Array Kit, Panel A (R&D Systems) according to manufacturer's procedures. Briefly, $1 \cdot 10^7$ tumor cells were seeded in 15 cm plates and grown for 3 d

(70-80% confluent). Supernatants were harvested and centrifuged at 300 g for 10 min, then immediately mixed with biotinylated detection Abs and probed onto nitrocellulose membranes (pre-spotted with 40 different capture Abs). The protein capture step was performed over night at 4°C while rocking. Following 3 washes, the captured cytokines and chemokines were visualized in duplicate using a chemiluminescence detection readout (1 min exposure).

Parabiosis and proliferation/recruitment studies

Six to eight week old CD45.1 and CD45.2 C57BL/6 female mice (Jackson Labs) were anesthetized with isoflurane and shaved at corresponding lateral sides. Matching skin incisions were made from the elbow to the knee of each mouse and the subcutaneous fascia were bluntly dissected to create about 0.5 cm of free skin. The olecranon and knee joints were attached by a mono-nylon 5.0 suture (Ethicon) and the dorsal and ventral skins were connected by continuous suture. The parabiont pair received $1 \cdot 10^5$ B16F10 tumor cells in 50 μ l of HBSS intradermally on the flank 10 d later. For proliferation and recruitment studies, mice were challenged with B16F10 tumors as above and received an intraperitoneal dose of BrdU (1mg) 2 d before euthanasia. Alternatively, tdLNs were stained *ex vivo* with the proliferation marker Ki67 (eBioscience).

Whole mount LN imaging

Liposome- or DT-treated mice were euthanized and LNs were carefully isolated from surrounding fat tissue. After fixation with 4% PFA (Alfa Aesar) for 1 h at 4°C, LNs were permeabilized/stained with 0.5% Triton X100 (Sigma), 10% Goat serum (Abcam), 2 μ g/ml (1:100 dilution) of both FcBlock and directly conjugated Abs (Biolegend) at 4°C overnight in 500 μ l of PBS, rocking. For imaging analyses we used the CD63-GFP genetic marker because the commercial mouse anti-human CD271 Ab, which detects dLNGFR, can yield non-specific immunofluorescence staining in murine samples. For secondary eGFP detection, monoclonal rat Ab against GFP (Life Technologies) was used at 10 μ g/ml (1:200 dilution) at 4°C overnight in 500 μ l of PBS while rocking. Then the LNs were washed 2 times in 5 ml of 0.5% Triton X100 (Sigma) and 10% Goat serum (Abcam) at 4°C overnight/overday in 500 μ l of in PBS while rocking. Finally, a secondary Alexa-488 anti-rat Ab (Life Technologies) was used at 4 μ g/ml (1:500 dilution) at 4°C for 24 h in 500 μ l of PBS while rocking. Before imaging, LNs were washed 2 times as above and whole-mounted on a slide within a pool of PBS contained with vacuum grease. A coverslip was gently placed on top in order to immobilize the LN. EGFP, Alexa-488, FITC and PE fluorochromes were visualized through multiphoton excitation using a DeepSee Ti:sapphire laser (Newport/Spectra-Physics) tuned to 920 nm. Depending on the experiment, different acquisition modalities were adopted:

- Single field of view, shallow volume: 30 optical sections with 1- μ m Z-spacing were acquired to provide image volumes of 30 μ m in depth and 614 x 614 μ m in width.
- Single field of view, deep volume: 200 optical sections with 2- μ m Z-spacing were acquired to provide image volumes 400 μ m in depth and 614 x 614 μ m in width.
- Whole LN sections: Multiple adjacent square optical sections were acquired with 15% overlap using the Atlas function of PrairieView (Bruker) to generate stitched high-resolution (20x) images encompassing the entire LN circumference.
- Deep Atlas: a combination of the above two imaging modalities (whole LN section and deep volumes).

Emitted fluorescence was detected with an Olympus 20x 0.95 NA objective on an Ultima IV multiphoton microscope (Bruker) through 460/50 (second harmonic generation),

525/50 (eGFP, Alexa488 or FITC), 595/50 (PE), and 660/40 band-pass filters and non-descanned detectors to generate 4-color images. Signal in the empty 660/40 channel was considered autofluorescence and subtracted from all other channels.

Image analysis

Depending on the acquisition modalities used (see above), the following image processing was performed:

- Single field of view, shallow or deep volume: images from multiple samples, multiple acquisitions per sample, were pre-processed in batches using RStudio. Operations performed in R were: channel subtraction, channel merge and file name formatting. Stack images were then projected in Fiji. Post-processing included noise removal (despeckle) and brightness/contrast normalization, i.e. same min-max value for all samples. In particular, to detect CD63-GFP⁺ tEVs a min-max values of 200-5000 was used for images from both PBS- and clodronate-liposome treatment groups.
- Whole LN sections: images from multiple samples, multiple acquisitions per sample, were pre-processed in batches using RStudio. Operations performed in R were: channel subtraction, channel merge and file name formatting. Image stitching was then performed in Fiji. Post-processing included noise removal (despeckle) and brightness/contrast normalization, i.e. same min-max value for all samples. ImageJ macro language was used to perform unbiased cell counting (for instance, Ki67⁺ and BrdU⁺ cells in parabiosis studies) in batches across the whole sample set. The auto-thresholding algorithm was selected after visual inspection of a sample image processed with all available algorithms to match the outcome with real signal from the relevant channel.
- Deep Atlas: images from a single deep atlas acquisition were imported in Fiji using the Grid/Collection stitching plugin and the XML file generated during acquisition. The resulting stack contained stitched images for all Z positions. Post-processing includes noise removal (despeckle) and average intensity Z projection. ImageJ macro language was used to perform unbiased particle counting (for instance, SCS Mø barrier area and tEV counting) in batches across the whole sample set. The auto-thresholding algorithm was selected after visual inspection of a sample image processed with all available algorithms to match the outcome with real signal from the relevant channel.

Western blot

tEV preparations were lysed (150 µl) by adding 10x RIPA buffer and 100x protein inhibitor/EDTA (Pierce). Samples were syringed (23G) 5 times, sonicated 10+10 seconds on ice 4 times, vortexed for a few seconds every min 5 times and centrifuged at 14,000 g for 15 min at 4°C to pellet-insoluble material. Protein concentration in supernatants was quantified using BCA, and 10 µg of protein were mixed with 4x loading dye (Pierce) and boiled in water bath for 5 min. Samples were then loaded on an SDS precast nitrocellulose gel (Life Tech.). The gels were run for 1 h at 200V, rinsed in distilled water and washed in SuperBlock (Pierce) for 1 h while rocking. After washing with TBS-Tween20 0.1% for 5 min 2 times while rocking, the gel was stained with both mouse anti-CRE mAb (Sigma) and rabbit anti-HSP90 mAb (Cellsignal) (both at a 1:2000 dilution) in TBS-Tween20 10% superBlock, 5 ml, overnight at 4°C while rocking. After washing with PBS-Tween20 0.05% for 5 min 3 times, while rocking, secondary detection was performed with HRP-conjugated goat anti-mouse (Abcam) at a 1:20,000 dilution, HRP goat anti-rabbit (Abcam) at a 1:20,000 dilution, in TBS-Tween20 5% nonfat dry milk in PBS-Tween20 0.05% for 1 h while rocking. The gels were washed with PBS-Tween20

0.05% while rocking (5 min, 3 times) and treated with supersignal reagent (Pierce) in 2 ml for 5 min at room temperature while rocking, then developed.

B cell depletion, IgG isolation and analysis

To deplete B cells, anti-CD20 Ab clone 5D2 (Genentech) was administered intraperitoneally (250 µg per mouse, one d before tumor challenge) once per week for 2 weeks. For IgG isolation, ~500 µl of blood was drawn by cardiac puncture. Coagulation was prevented by EDTA. Plasma was obtained by centrifugation at 2,000 g for 15 min. IgGs were purified using a protein G based kit (Pierce) and quantified with the Bradford assay. The purity of the undiluted IgG preparations was examined on an SDS gel by Coomassie staining after methanol/acetic acid destain. Purified IgGs (25 µg) were retro-orbitally injected in mice simultaneously with intradermal B16F10 tumor challenge. For tEV pulldown, before IgGs elution from protein G columns, an equal amount of PKH67⁺ tEVs was loaded on the columns, which were then washed 3 times. IgGs were eluted, and the PKH67 fluorescence was measured in a plate reader against a standard curve of the initial PKH67⁺ tEVs.

Statistics

Results were expressed as mean±SEM. GraphPad Prism 6 was used for all statistical analyses. Statistical tests with normally distributed variables included 2-tailed Student's *t* test and 1-way ANOVA followed by Bonferroni's multiple comparison test. When variables were not normally distributed, we performed non-parametric Mann-Whitney or Kruskal–Wallis tests. P values < 0.05 were considered significant.

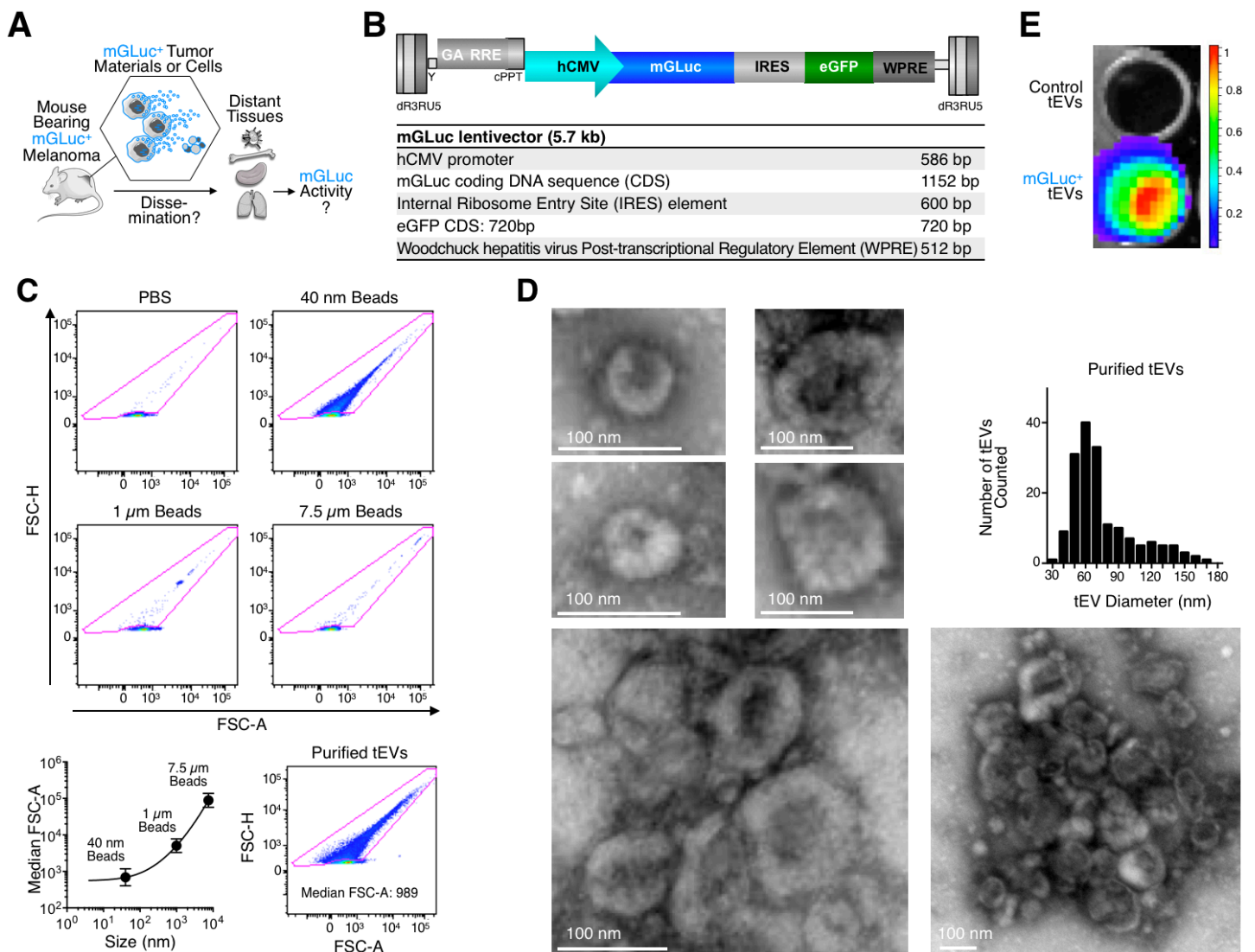


Fig. S1. Characteristics of mGLuc⁺ B16F10 tEVs. (A) Experimental outline to define whole-body dissemination of B16F10 melanoma-derived materials. (B) Schematic of the proviral lentiviral vector used to produce mGLuc⁺ B16F10 tumor cells. (C) Flow cytometry based analysis of size standards and of tEVs purified from B16F10 cell culture supernatants. The PBS sample in the top left panel shows electronic noise or contamination above the lowest possible detection threshold. Regression analysis between size of standard beads and Forward Scatter Area (FSC-A) median is shown in the bottom left panel. (D) Representative transmission electron microscopy images of tEVs purified from B16F10 cell culture supernatants. The four top-left panels show individual tEVs with modal size of 60-100 nm, whereas the two bottom panels show tEV clusters. The top right panel shows tEV size distribution from all preparations tested (n = 8). (E) tEV luciferase activity of mGLuc⁻ (upper well) and mGLuc⁺ (lower well) B16F10 cell culture supernatants. mGLuc = membrane-bound Gaussia Luciferase; tEVs = tumor-derived extracellular vesicles. Taken together these data indicate that tEVs derived from mGLuc⁺ B16F10 tumors have the expected size of extracellular microvesicles and are efficiently detected by bioluminescence imaging. In contrast to secreted GLuc, mGLuc confers specific luminescence activity to tEV preparations, suggesting that mGLuc indeed is not secreted freely, but rather released in tEVs (10). These data also indicate that we can track endogenously produced tEVs without *in vitro* manipulation.

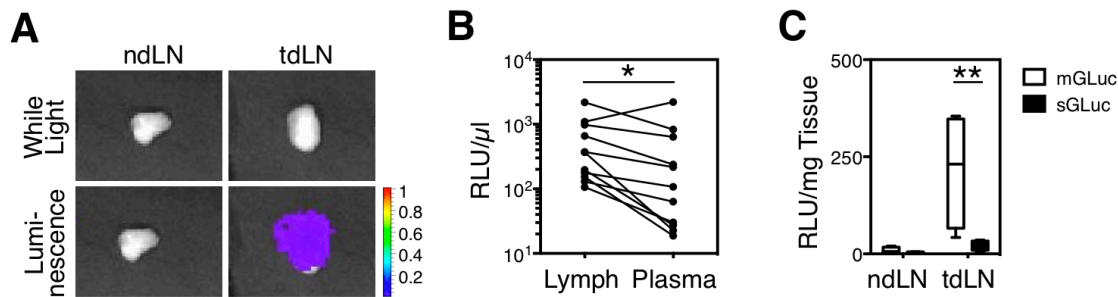


Fig. S2. Detection of mGLuc⁺ tEVs in tdLNs and lymph. (A) Detection of mGLuc⁺ activity in tdLNs. Representative white light images (top) and bioluminescence/white light image overlays (bottom) of ndLN (left) and tdLN (right) from the same mouse. Undetectable luminescence signal is not pseudo-colored. (B) Bioluminescence activity per μ l of lymph or plasma from mice bearing mGLuc⁺ B16F10 tumors (2 independent experiments; n = 11). (C) Bioluminescence activity per mg tissue in ndLN and tdLN lysates from mice bearing B16F10 expressing either membrane-bound GLuc (mGLuc) or secreted GLuc (sGLuc). (n = 4). *P < 0.05; **P < 0.01; Wilcoxon matched-pairs signed rank test for panel B; Two-way ANOVA with Sidak's multiple comparisons test for panel C. RLU = relative luminescence units.

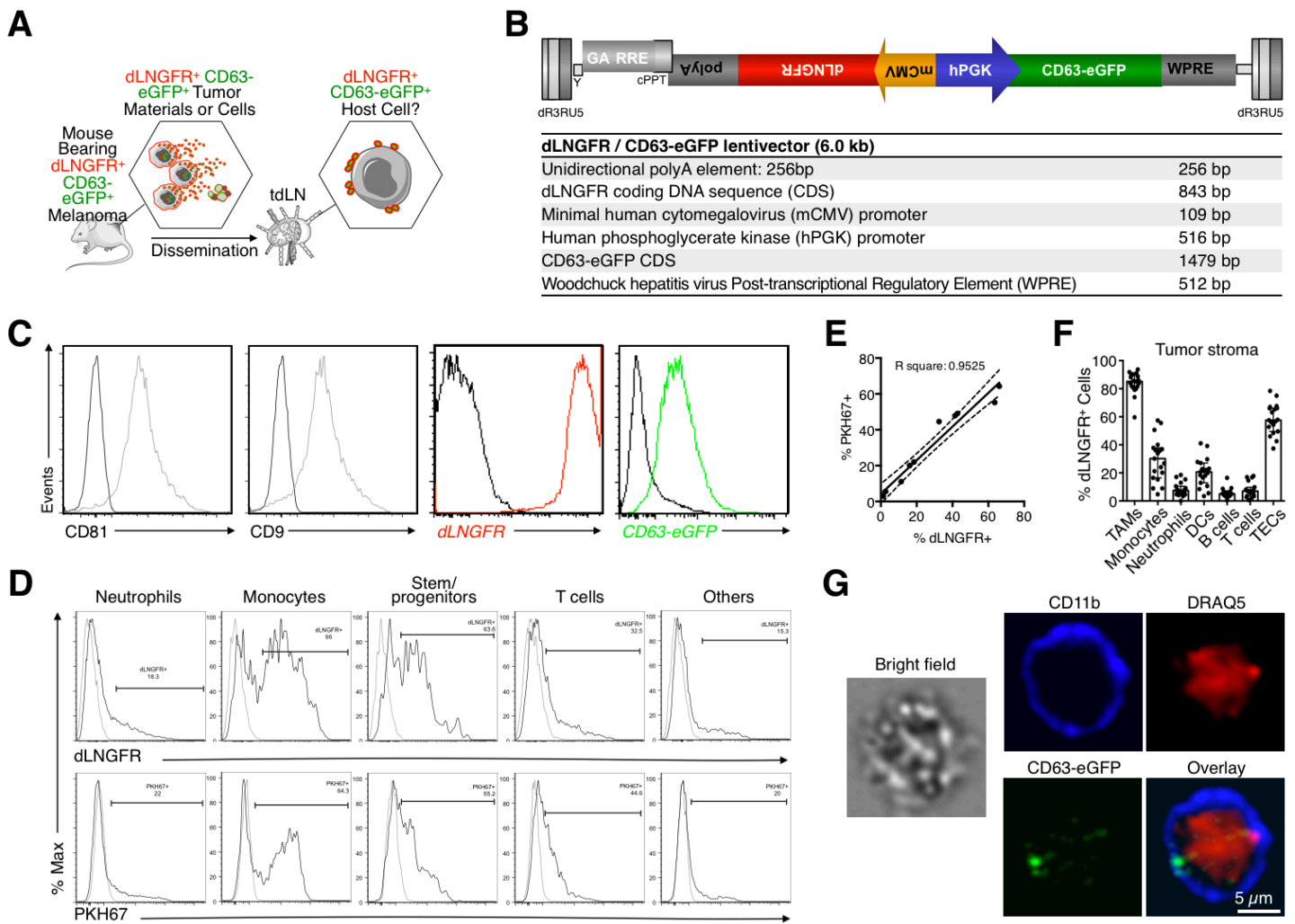


Fig. S3. Characteristics of dLNGFR⁺ CD63-eGFP⁺ B16F10 tEVs. (A) Experimental outline to uncover host cells binding tumor-derived materials. (B) Schematic of the proviral lentiviral vector used to produce dLNGFR⁺ CD63-eGFP⁺ B16F10 tumor cells. (C) Flow cytometry based analysis of tEVs purified from dLNGFR⁺ CD63-eGFP⁺ B16F10 cell culture supernatants and labeled with Abs against either CD81, CD9 or dLNGFR, or detected directly based on eGFP fluorescence (left to right, respectively). Control overlays performed by Ab staining of tEV-free PBS. (D) Flow cytometry based analysis of primary bone marrow cell subsets incubated with either dLNGFR⁺ tEVs (upper panels) or tEVs labeled with PKH67 ex vivo. Light grey histograms are for control samples that were not incubated with tEVs (n = 2). (E) Correlation analysis between dLNGFR⁺ and PKH67⁺ fractions for each primary bone marrow cell subset shown in C). (F) Ex vivo flow cytometry of dLNGFR⁺ B16F10 tumor stroma to quantify the percent of indicated host cells that are also dLNGFR⁺ (2 independent experiments, n > 10). (G) Ex vivo imaging flow cytometry of a representative CD11b⁺ macrophage stained positive for CD63-eGFP and retrieved from a CD63-eGFP⁺ B16F10 tumor site. DRAQ5 counterstains nuclear content (n = 3). DCs = dendritic cells; dLNGFR = truncated receptor for nerve growth factor; eGFP = enhanced green fluorescent protein; TECs = tumor endothelial cells; tEV = tumor-derived extracellular vesicles. Taken together these data validate that tEVs derived from dLNGFR⁺ CD63-eGFP⁺ B16F10 tumors express both dLNGFR and CD63-eGFP reporters and bind various immune cell types *ex vivo* as efficiently as B16F10-derived tEVs exogenously labeled with PKH67, a standard dye for fluorescent tEV tracing (4). Additionally, flow cytometry and imaging cytometry *ex vivo* confirm that tEVs bind tumor-infiltrating host cells, including tumor-associated macrophages (TAMs).

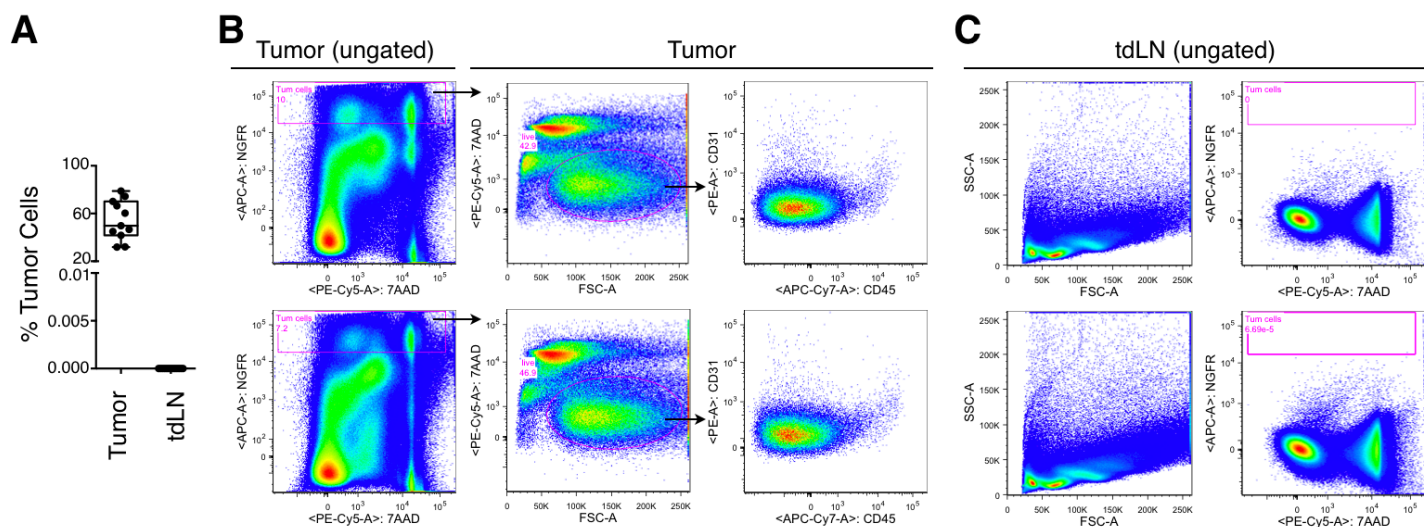


Fig. S4. Absence of tumor cells in tdLNs by flow cytometry. (A) Percent of tumor cells (defined as 7AAD⁻ CD45⁻ dLNGFR^{HIGH}) in tumor stroma and tdLNs from mice bearing CD63-GFP+ dLNGFR+ B16F10 cells (2 independent experiments, n > 10). (B) Flow cytometry plots showing dLNGFR expression level in tumor cells, gated first as dLNGFR^{HIGH} cells (left most panels), then as viable 7AAD⁻ cells (middle panels). Resulting gate contains cells negative for both the hemopoietic marker CD45 and for the endothelial marker CD31 (right most panels). Two representative samples are shown, one per row. (C) Flow cytometry plots showing absence of dLNGFR⁺⁺⁺ tumor cells in ungated tdLN samples. Two representative samples are shown, one per row. tdLN = tumor-draining lymph node. tEV = tumor-derived extracellular vesicles.

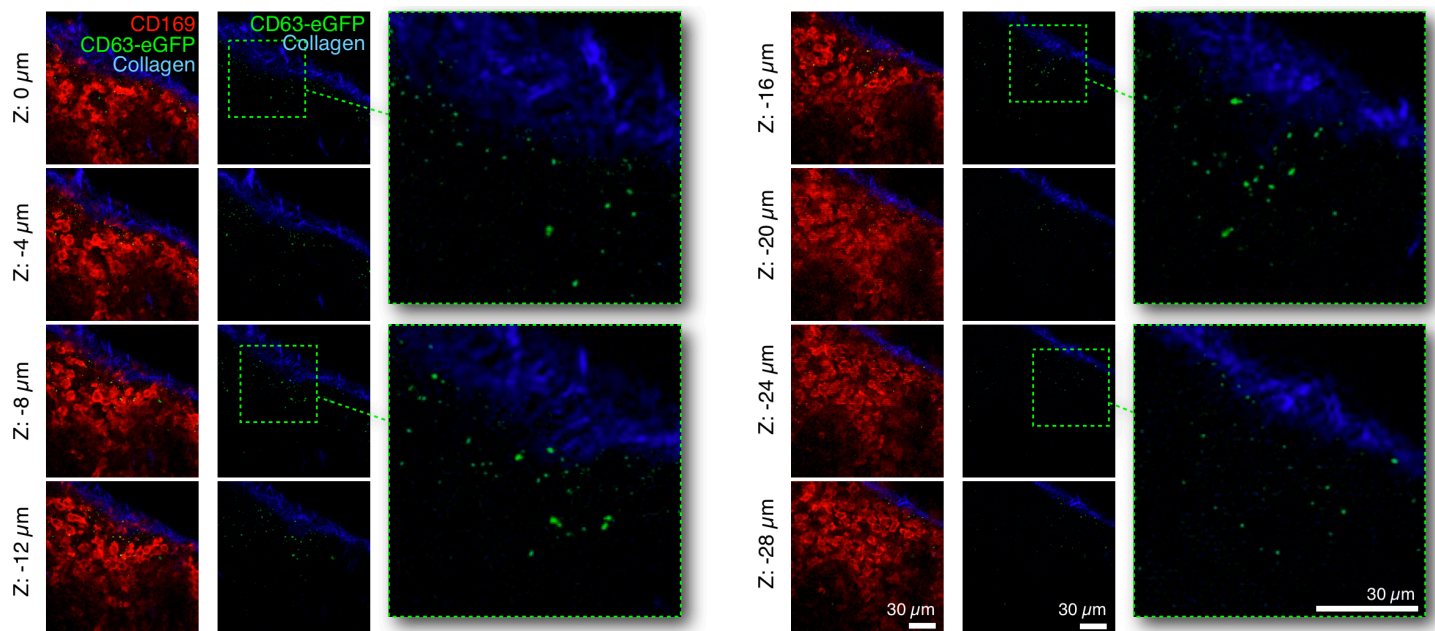


Fig. S5. Absence of tumor cells in tdLNs by imaging. Multiphoton microscopy of tdLN from mice bearing CD63-GFP+ dLNGFR+ B16F10 cells. tdLNs were stained for GFP (green; to reveal tEVs) and CD169 (red). LN capsule is in blue. Serial optical sections 4 μm apart are shown. (2 independent experiments, n = 6). tdLN = tumor-draining lymph node.

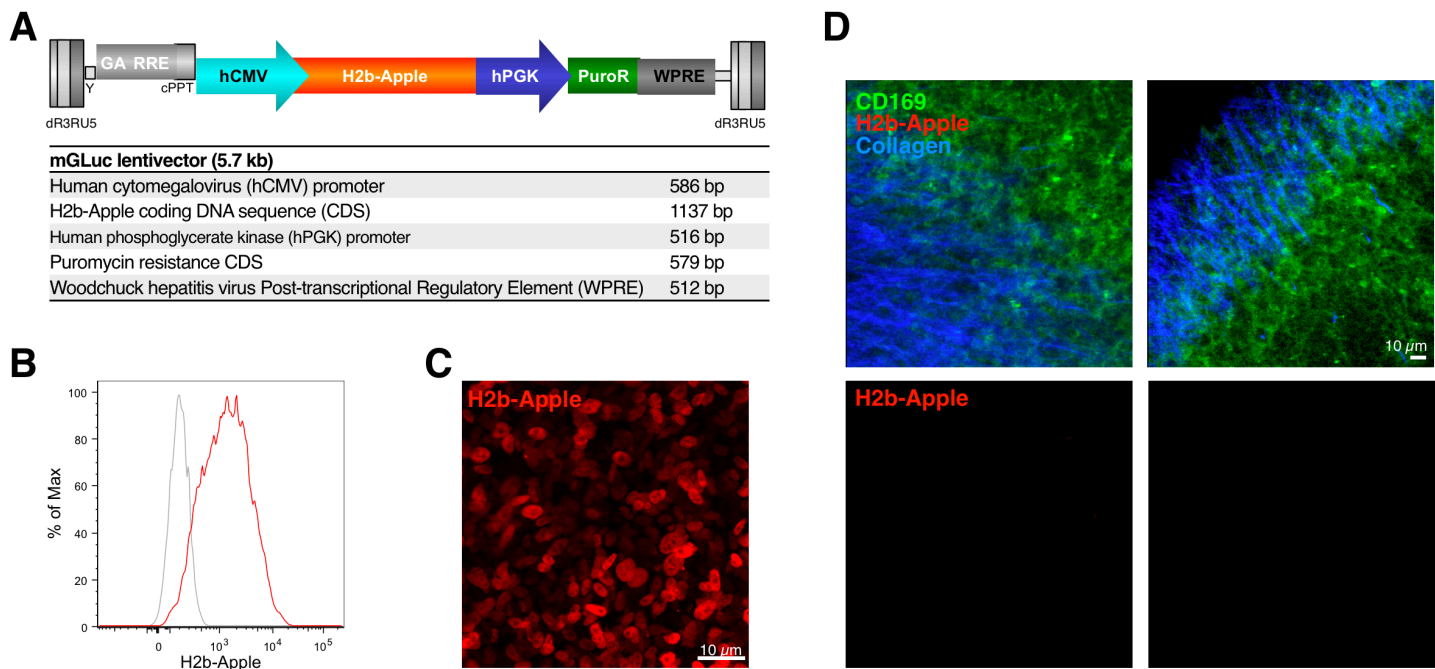


Fig. S6. In vivo tracking of dead tumor cells and apoptotic bodies using H2b-Apple⁺ B16F10 tumors. (A) Schematic of the proviral lentiviral vector used to produce H2B-Apple⁺ B16F10 tumor cells (no Puromycin selection has been used). Flow cytometry analysis (B) and fluorescence microscopy imaging (C) of cultured H2B-Apple⁺ B16F10 tumor cells. (D) Two representative micrographs (top panels) of tdLN from H2B-Apple⁺ B16F10 bearing mice. tdLNs were stained for CD169 (green). H2B-Apple direct fluorescence is in red, LN capsule (collagen visualized by second harmonic generation) is in blue. Bottom panels show red channel only. Each panel represents a 30 μm deep volume projected on the Z-axis ($n = 4$). tdLN = tumor-draining lymph node.

Primary + secondary mAb: (I) Rabbit anti-GFP + (II) anti-rabbit Alexa-488

Secondary mAb only (anti-rabbit Alexa-488; no rabbit anti-GFP)

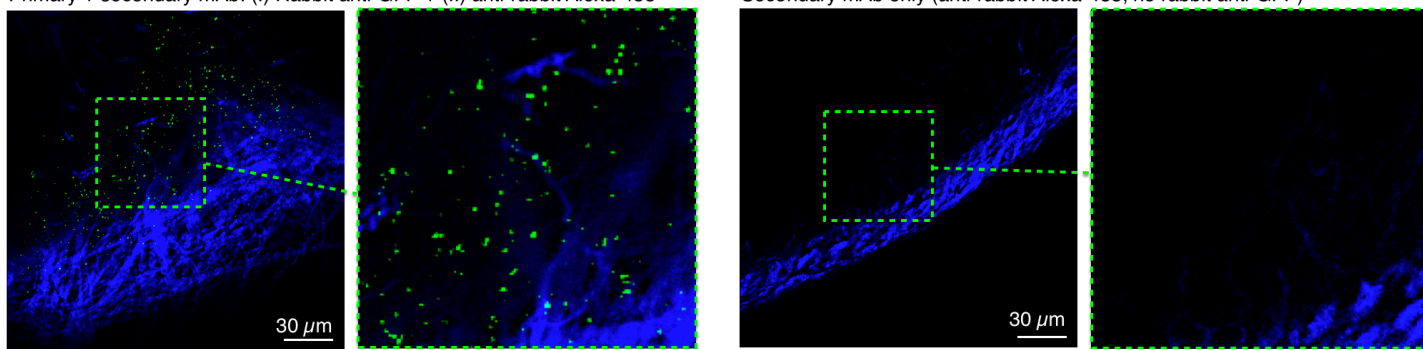


Fig. S8. Validation of eGFP staining specificity for tEVs. Since flow cytometry requires tissue preparation that can favor SCS macrophage fragmentation (36), we independently assessed tEV distribution in whole tdLNs by multiphoton microscopy. Here, eGFP (left panels) and control (right panels) staining of tdLNs from mice carrying CD63-eGFP⁺ B16F10 melanomas are shown (n = 3).

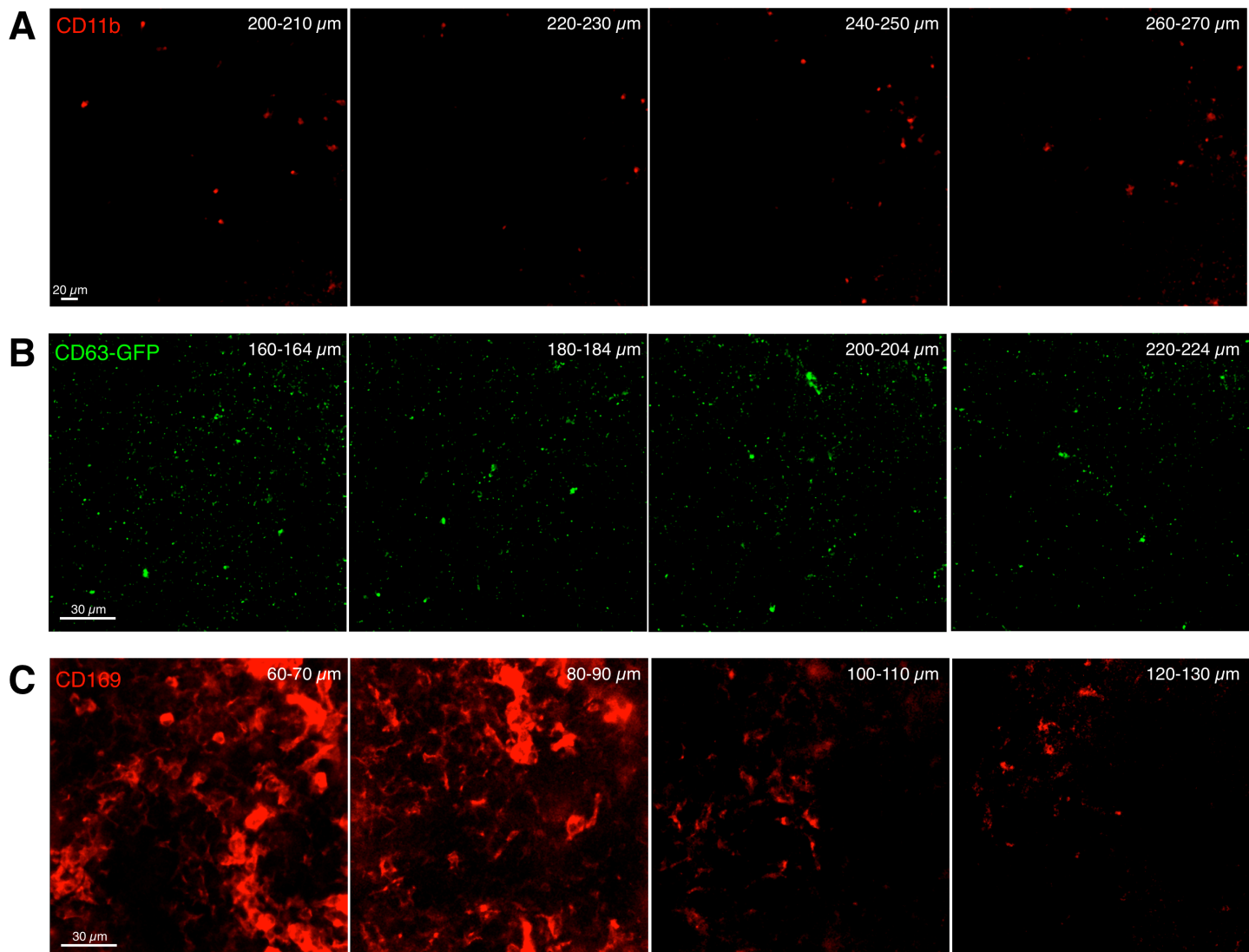


Fig. S9. Validation of Ab staining protocol for whole mount LN preparations. Multiphoton microscopy analysis of tdLN from mice challenged with CD63-GFP⁺ B16F10 melanoma cells. Images represent Z-axis projected sections of the indicated range below the LN capsule for 3 different Abs: (A) anti-CD11b; (B) anti-GFP (clodronate-liposome treated mice); (C) anti-CD169. Here, CD63-GFP⁺ tEVs were detected deep into the LN because mice were treated with clodronate liposomes to deplete SCS macrophages. tdLN = tumor-draining lymph node (n = 3).

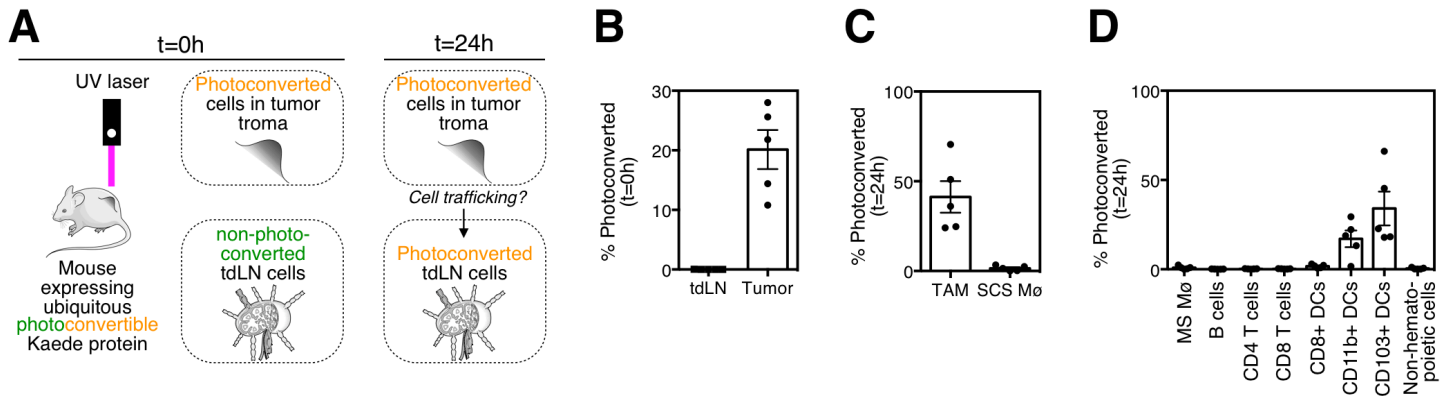


Fig. S10. Flow cytometry-based tracking of cell migration from tumor stroma to tdLN using a photoconvertible fluorescent protein. (A) Experimental outline to follow migration of tumor-associated host cells from tumor stroma to tdLN. (B) Fraction of cells photoconverted in the tumor right after UV laser treatment (time = 0h) and confirmation that tdLN cells are not photoconverted at this time point (n = 5). (C) Flow cytometry based quantification of photoconverted SCS Mø in tdLNs at time = 24h. Control data for TAMs obtained at the same time point are shown (n = 5). (D) Flow cytometry based quantification of photoconversion among other cell types in tdLNs at time = 24h. DC = dendritic cells; Mø = macrophage; MS = medullary sinus; mGLuc = membrane-bound Gaussia Luciferase; RLU = Relative luminescence unit; SCS = subcapsular sinus; TAM = tumor-associated macrophages; tdLN = tumor-draining lymph node.

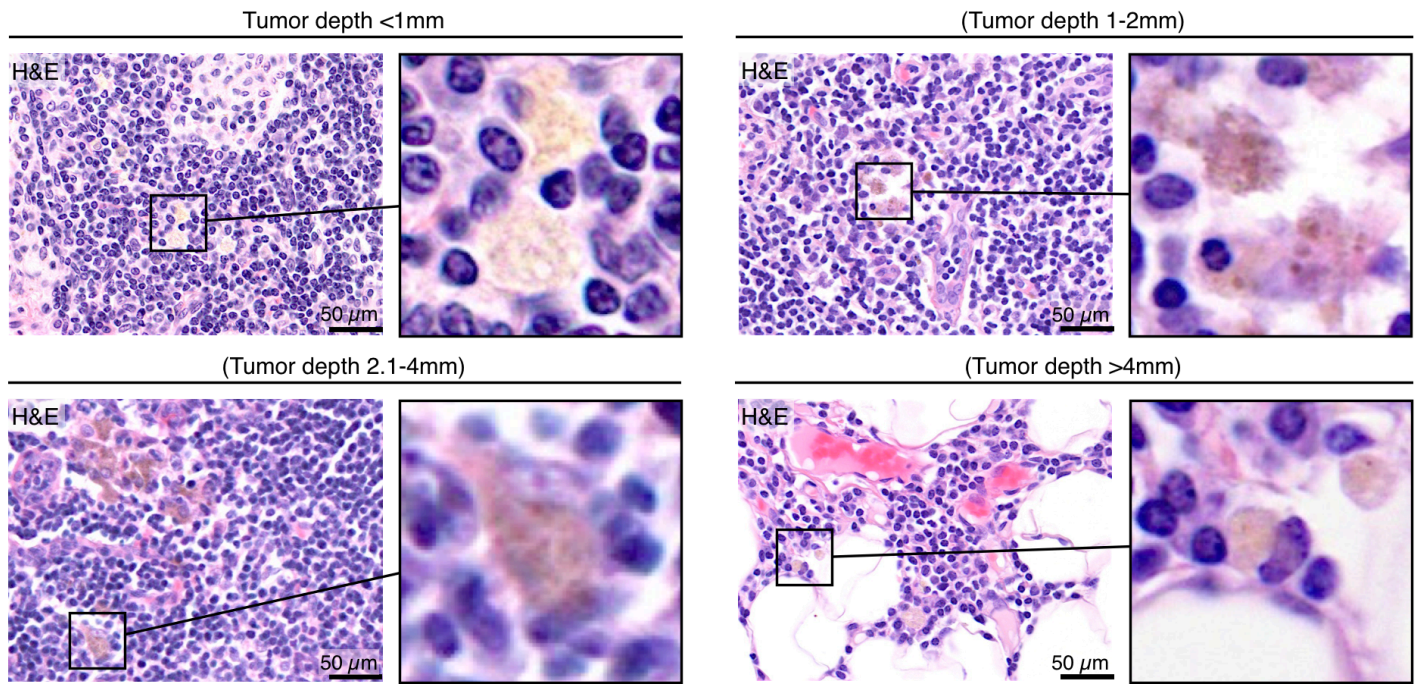


Fig. S11. Hematoxylin and eosin (H&E) staining of human melanoma-free (i.e. stage N0) sentinel LNs. Representative examples for different tumor stages (according to the American Joint Committee on Cancer guidelines).

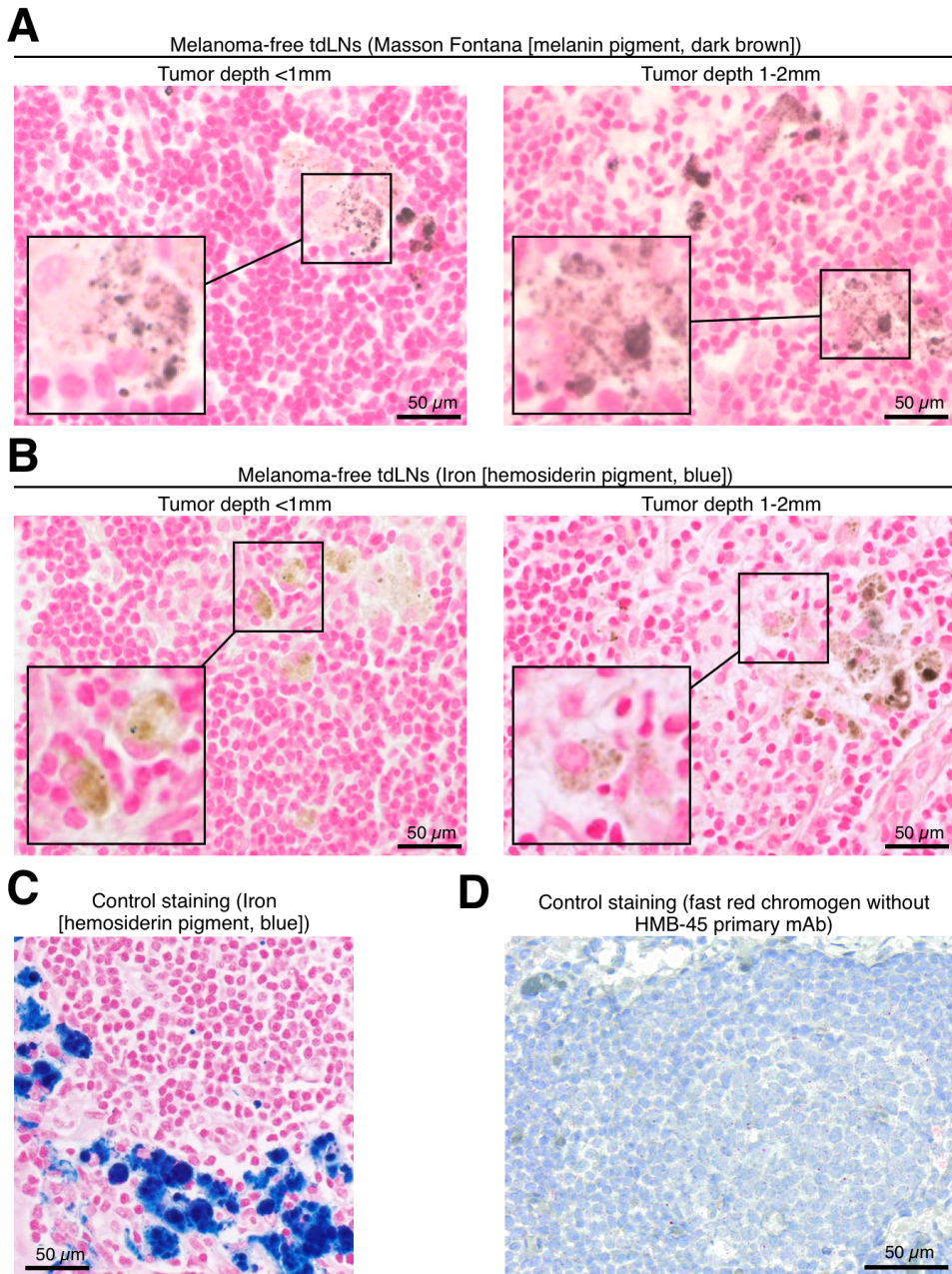


Fig. S12. Melanin pigment staining (Masson-Fontana) and hemosiderin pigment staining (iron) of human melanoma-free (i.e. stage N0) sentinel LNs. To distinguish melanin from hemosiderin pigment, we performed Masson Fontana staining for melanin and Iron staining for hemosiderin. **(A)** Positive Masson-Fontana staining (brown) in macrophage-like cells. **(B)** Negative iron staining (blue) in macrophage-like cells. **(C)** Positive control for iron staining (blue) in LN siderophages. **(D)** Negative control for HMB45 staining. Here, no primary HMB45 mAb was used before addition of the fast red chromogen. These analyses confirm the presence of melanin pigments in CF-SLN macrophages, as defined by histological examination.

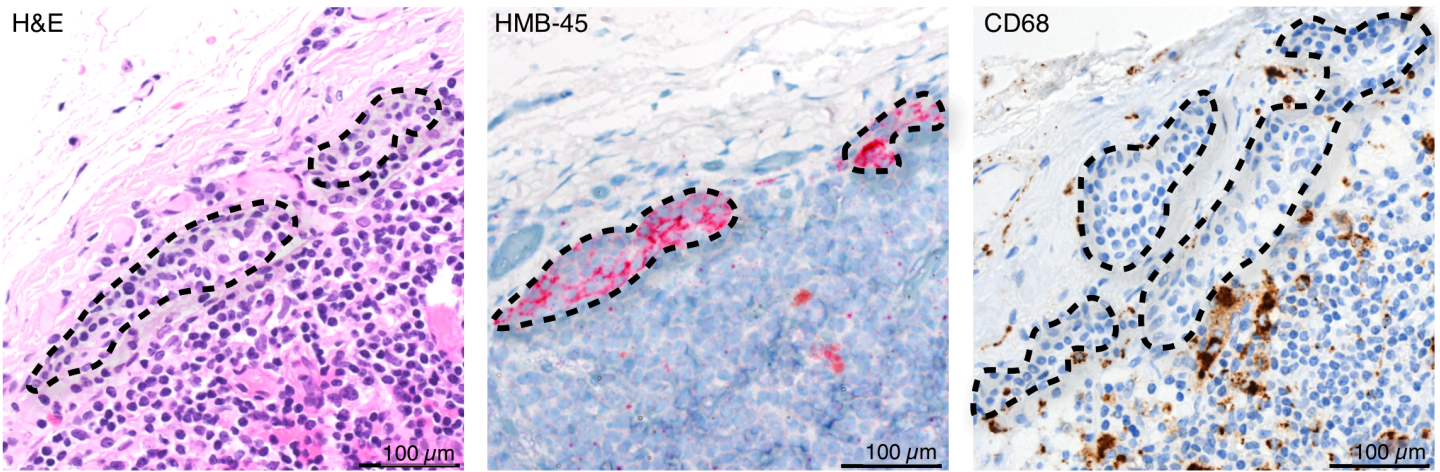


Fig. S13. Characteristics of sentinel LN micro-metastases in human melanoma. A Sentinel LN containing sub-capsular micro-metastases (i.e. stage N1; dashed contours) was stained for hematoxylin and eosin (H&E, left), melanoma marker PMEL (clone HMB-45, center) and macrophage marker CD68 (right). Invading melanoma cells (highlighted with dashed lines) were defined by morphology and as HMB-45⁺. These analyses also indicated that the HMB-45 staining was more intense in melanoma cells than in macrophages.

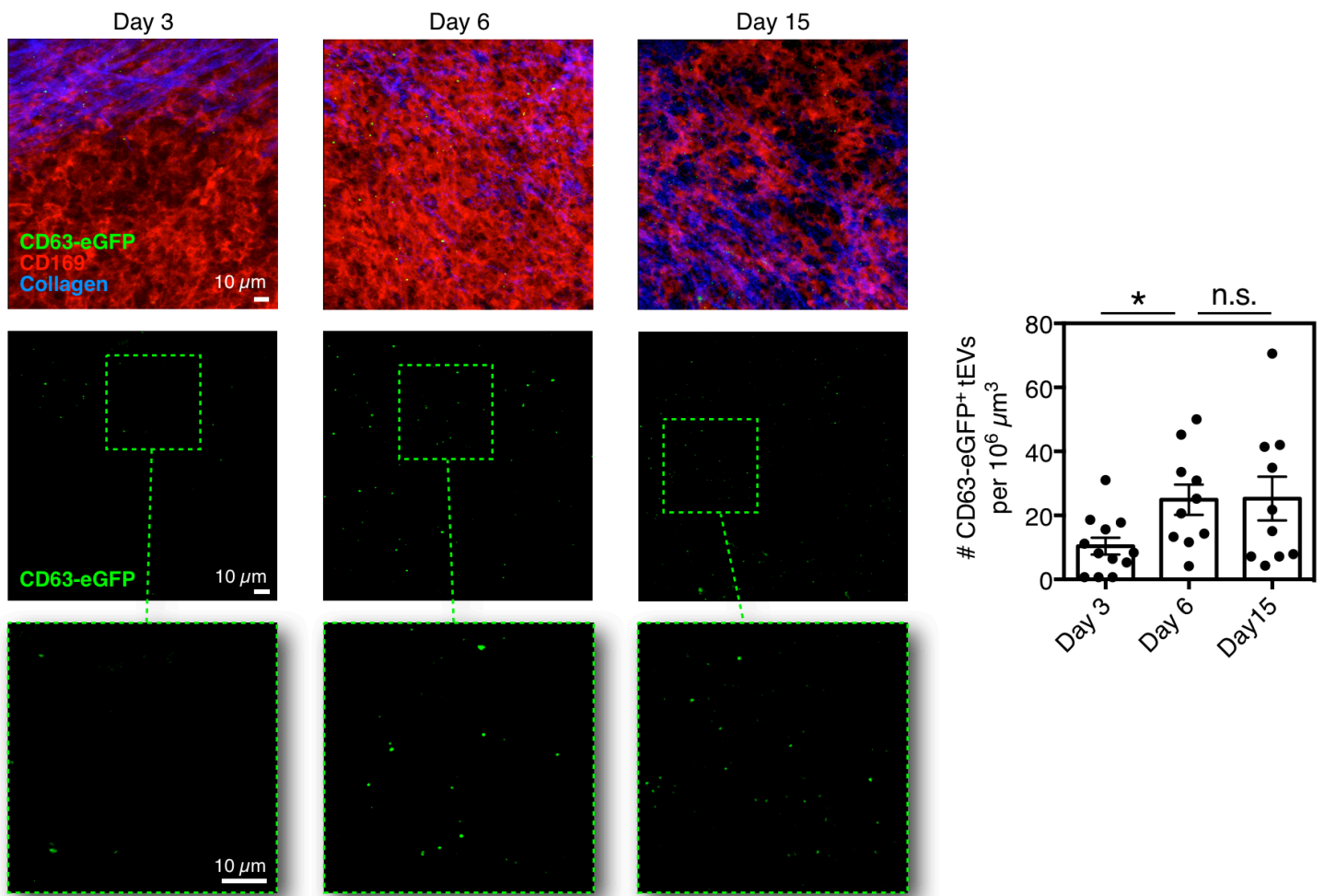


Fig. S14. Time course analysis of tEV accumulation in tdLNs. Multiphoton microscopy based quantification of tEV accumulation in tdLNs on d 3, 6 and 15 after intradermal injection of CD63-eGFP⁺ dLNGFR⁺ B16F10 cells. tdLNs are stained for CD63-eGFP (green) and CD169 (red). LN capsule (collagen) is in blue (n = 2-3). Top row shows 3 color merge pictures, middle and bottom rows show GFP only channel. *P < 0.05; n.s. = not significant; Mann Whitney test. tdLN = tumor-draining lymph node.

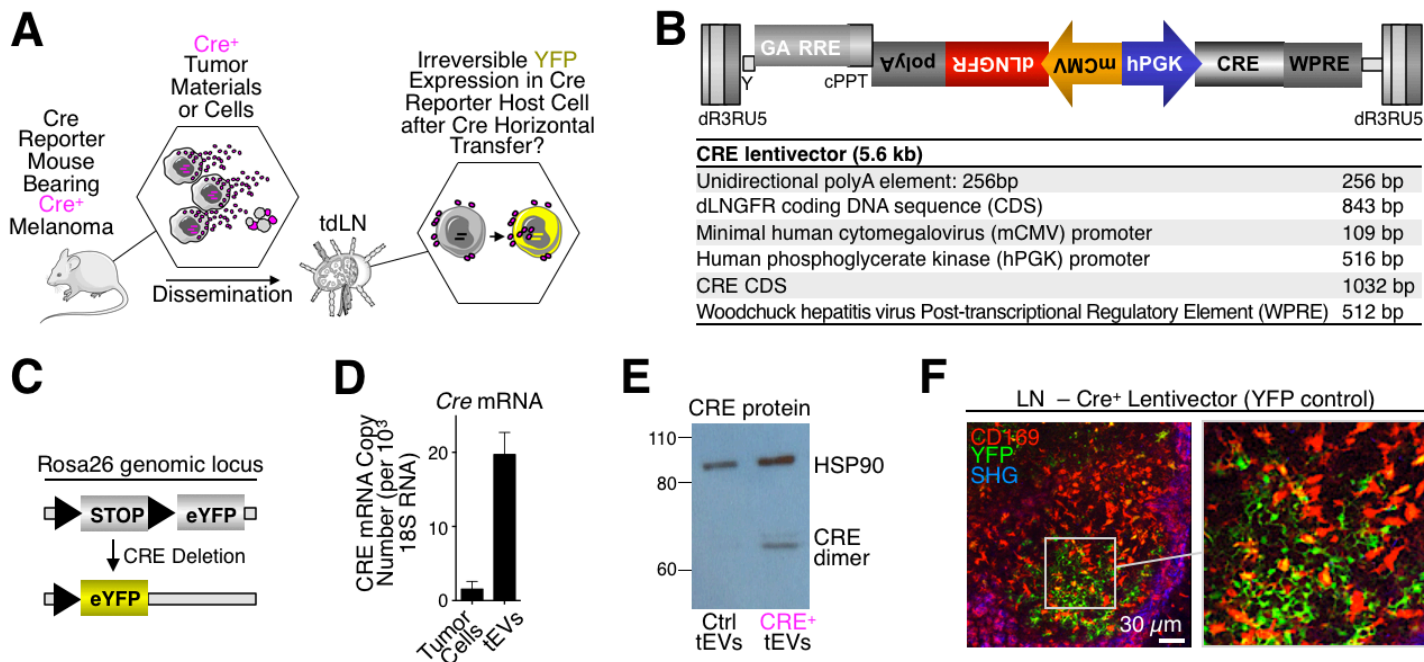


Fig. S15. Study of horizontal tEV transfer and characteristics of Cre⁺ B16F10 tEVs. (A) Experimental outline to study horizontal transfer of tEV cargo. (B) Schematic of the proviral lentiviral vector used to produce Cre⁺ B16F10 tumor cells. (C) Schematic of the Rosa26 genomic locus present in the Cre-reporter mice bearing Cre⁺ B16F10 tumor cells. (D) qPCR quantification of *Cre* mRNA from either Cre⁺ B16F10 tumor cells or Cre⁺ B16F10-derived tEVs. (n = 3). (E) CRE and HSP90 Western blot of tEVs purified from either control B16F10 or Cre⁺ B16F10 cells. (n = 3). (F) Multiphoton micrographs of LNs upon local injection of Cre⁺ lentivectors (n = 2). Panels C and D confirm that tEVs from B16F10–Cre⁺ melanoma cells contain both *Cre* mRNA and Cre protein. Panel F shows that intradermally injecting a control Cre-coding lentivector into tumor-free Cre-reporter mice induced YFP expression in CD169⁺ SCS macrophages, demonstrating these cells' ability to switch on YFP expression and multiphoton microscopy's capacity to detect SCS YFP⁺ macrophages and Cre-activated cells.

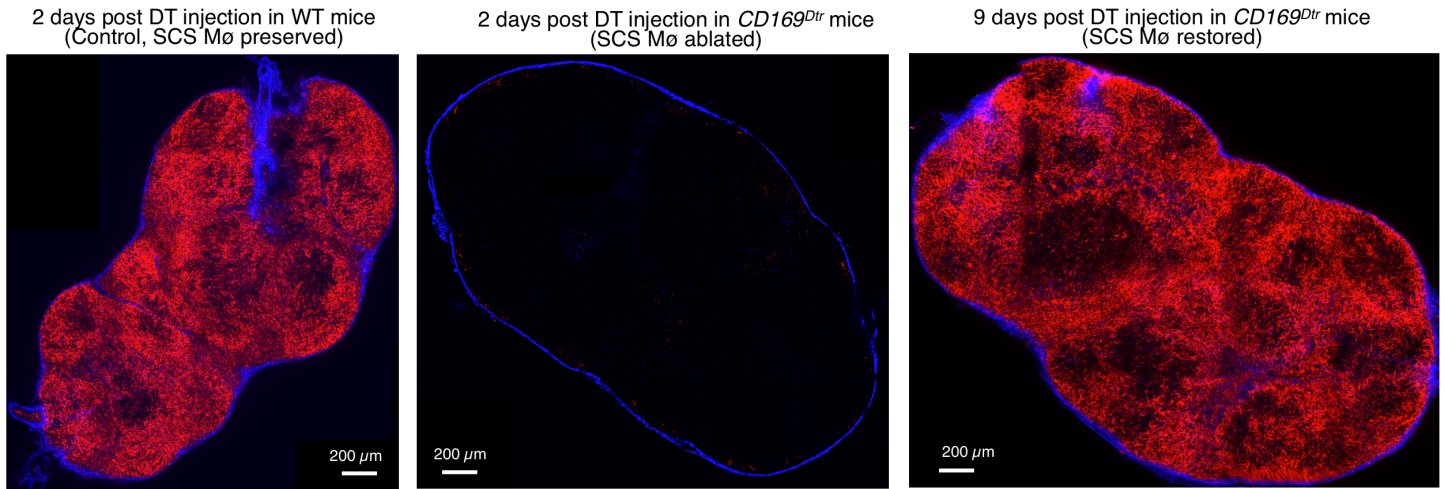


Fig. S16. CD169⁺ SCS macrophage depletion with Diphtheria toxin in Cd169^{Dtr/Wt} knockin mice. Multiphoton micrographs of tdLN whole mounts obtained from WT mice (left), Cd169^{Dtr/Wt} knockin mice injected 2 d earlier (center) and Cd169^{Dtr/Wt} knockin mice injected 9 d earlier (right); (n = 3) . Images represent a single optical section of compressed, entire LNs. tdLN were stained with anti-CD169 mAb (red). Second harmonic generation (SHG), shown in blue, identifies the LN capsule. DT = Diphtheria toxin; Mø = macrophages; tdLN = tumor-draining lymph node; SCS = sub-capsular sinus.

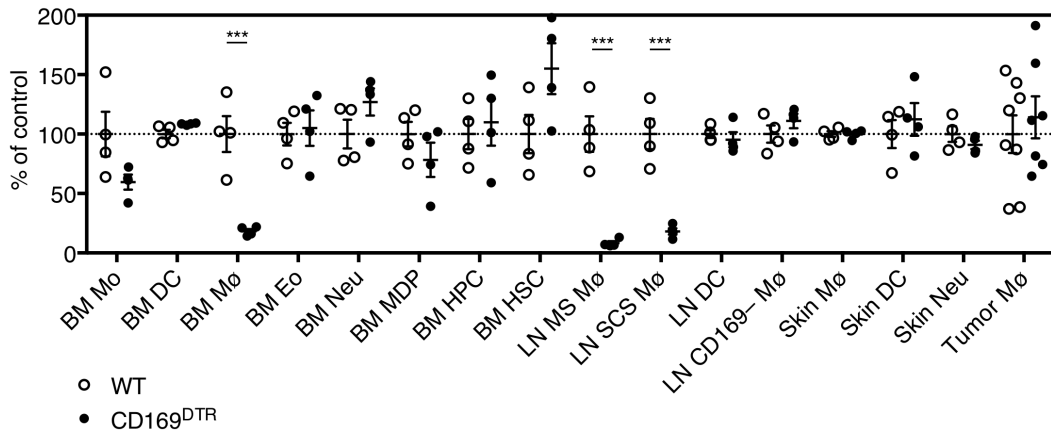


Fig. S17. CD169⁺ macrophage depletion with Diphtheria toxin (DT). Flow cytometry based quantification of cell depletion after intraperitoneal DT administration (500 ng, 2 d earlier) in WT or Cd169^{Dtr/Wt} mice (n = 4). Results are normalized to control (WT) mice. BM = bone marrow; DC = dendritic cells; Eo = eosinophils; HSC = hemopoietic stem cells; LN = lymph node; MDP = monocyte-DC progenitors; HPC = hemopoietic progenitor cells; LN = lymph node; Mø = macrophages; MS = medullary sinus; Mo = monocytes; Neu = neutrophils; SCS = sub-capsular sinus. ***P < 0.001; Two-way ANOVA with Sidak's multiple comparisons test.

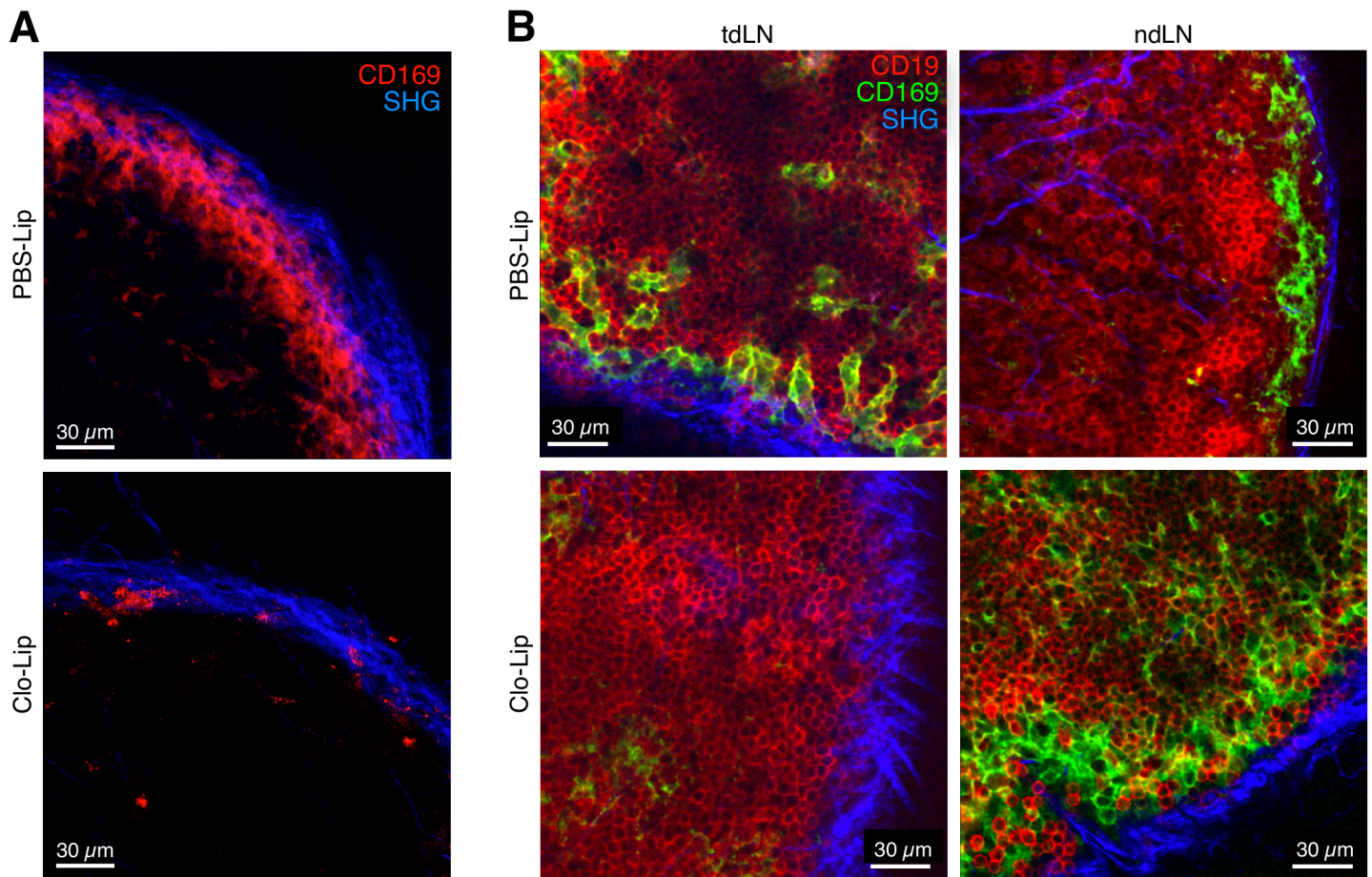


Fig. S18. Specificity of CD169⁺ SCS macrophage depletion with Clo-Lip. (A) Multiphoton micrographs of tdLN whole mounts obtained from mice subcutaneously treated with PBS-Lip (top) or Clo-Lip (bottom) and stained with anti-CD169 mAb (red). Second harmonic generation (SHG), shown in blue, identifies the LN capsule ($n = 3$). (B) Multiphoton micrographs of tdLNs (left) and ndLNs (right) from mice subcutaneously treated with PBS-Lip (top) or Clo-Lip (bottom) and stained with anti-CD169 (green) and anti-CD19 (red) mAb. Second harmonic generation (SHG) is shown in blue ($n = 3$). Clo-Lip = clodronate liposomes; ndLN = non-draining lymph node; PBS-Lip = PBS-loaded liposomes; tdLN = tumor-draining lymph node.

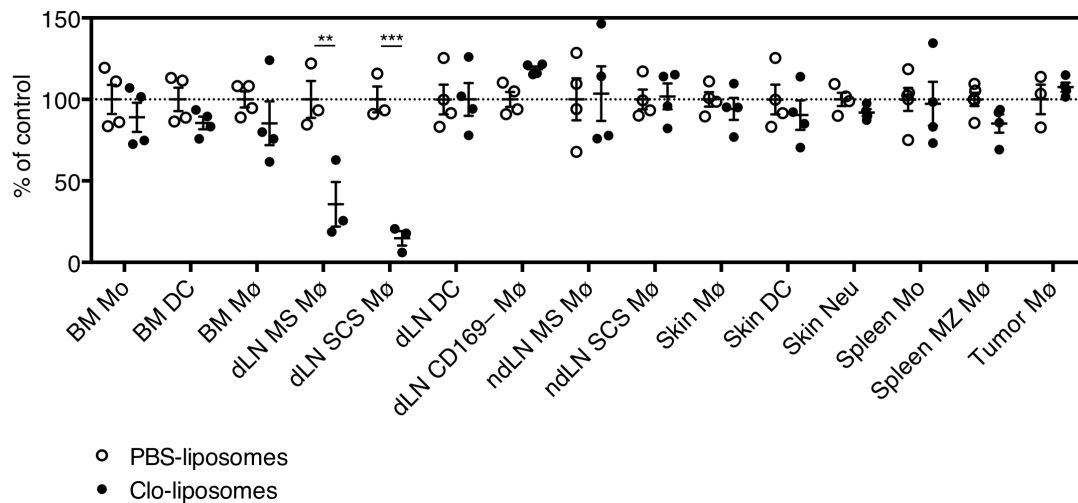


Fig. S19. CD169⁺ macrophage depletion with clodronate-liposomes. Flow cytometry based quantification of cell depletion after subcutaneous PBS- or Clodronate-liposome administration (50 μ l, calf, 6 d earlier, n = 3-4). Results are normalized to control (PBS-liposome treated) mice. BM = bone marrow; DC = dendritic cells; dLN = draining lymph node; Eo = eosinophils; HSC = hemopoietic stem cells; LN = lymph node; MDP = monocyte-DC progenitors; HPC = hemopoietic progenitor cells; Mø = macrophages; MS = medullary sinus; Mo = monocytes; MZ = marginal zone; Neu = neutrophils; ndLN = nondraining lymph node; SCS = sub-capsular sinus. **P < 0.01; ***P < 0.001; Two-way ANOVA with Sidak's multiple comparisons test.

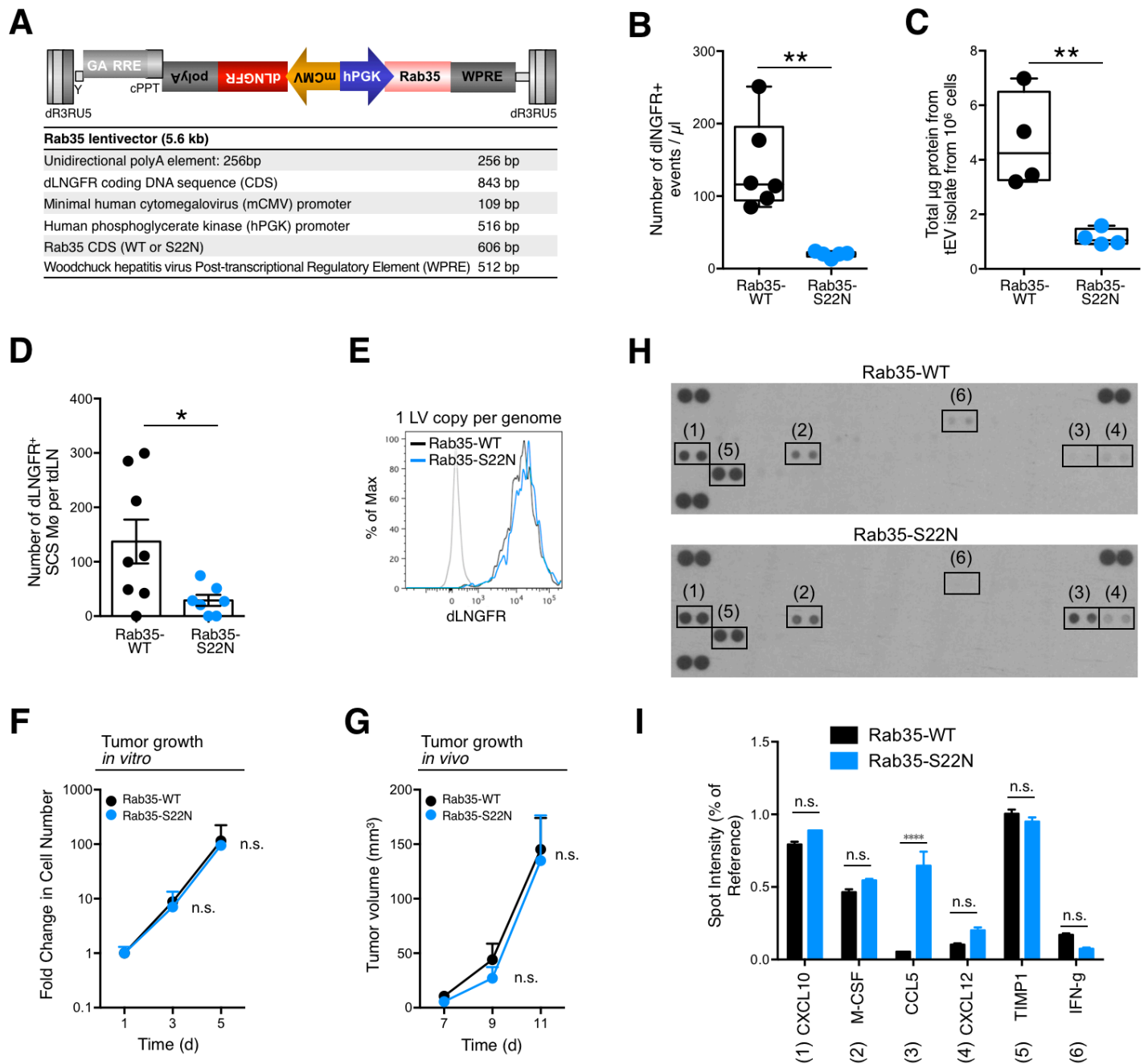


Fig. S20. Validation of a genetic approach to block tEV secretion in vivo. (A) Schematic of the proviral lentiviral vector used to generate Rab35^{WT} or Rab35^{S22N} expressing B16F10 tumor cells (tumor cells carry one copy per genome of the lentivector). (B) Flow cytometry-based quantification of dLNGFR⁺ tEVs produced by Rab35^{WT} and Rab35^{S22N} B16F10 tumor cells *in vitro*. Cell culture supernatants containing dLNGFR⁺ tEVs were obtained from the same number of Rab35 wild-type or Rab35 mutant tumor cells. Data representative of two independent experiments. (C) Quantification of total protein content in concentrated tEV preparations from cell culture supernatants and from the same number of tumor cells. Data representative of two independent experiments. (D) Flow cytometry-based quantification of tEV⁺ SCS macrophages in tDLNs from mice bearing Rab35^{WT} or Rab35^{S22N} expressing B16F10 melanomas. (E) Flow cytometry-based detection of dLNGFR expression by Rab35^{WT} and Rab35^{S22N} B16F10 tumor cells. (F) Rab35^{WT} and Rab35^{S22N} B16F10 tumor cell growth *in vitro*. Fold change in cell number of the two tumor cell lines cultured *in vitro*. Data are relative to cell counts measured on d 1. (n = 5-7), representative of two independent experiments. (G) Rab35^{WT} and Rab35^{S22N} B16F10 tumor cell growth *in vivo*. Tumor cells were inoculated into wild-type mice on d 0. (n = 5-7). Data are representative of two independent experiments. (H-I) Rab35^{WT} and Rab35^{S22N} B16F10 tumor cell cytokine and

chemokine secretory profiles. Cell culture supernatants were assayed for 40 cytokine and chemokine protein content using a proteome profiler cytokine array (H). Maximum intensity of detectable spots were normalized to the reference spots set to 1 (I). SCS = sub-capsular sinus; tdLN = tumor-draining lymph node. n.s., not significant. *P < 0.05; **P < 0.01; Mann Whitney test for panels B-D; Two-way ANOVA with Sidak's multiple comparisons test for panels F-I. Taken together, these data confirm reduced tEV release by Rab35 mutant tumor cells both *in vitro* and *in vivo*. They also indicate unaltered dLNGFR surface expression by the mutant cells, preserved growth of the mutant tumor cells both *in vitro* and *in vivo* in the presence of CD169⁺ LN macrophages, and largely overlapping cytokine/chemokine production profiles for Rab35 mutant and wild-type tumor cells (both tumor cells produced 39 of 40 cytokines at similar levels, whereas Rab35 mutant cells produced more CCL5). Since CCL5 can favor melanoma progression (37), it is unlikely to prevent Rab35 mutant tumor growth following SCS macrophage depletion *in vivo*.

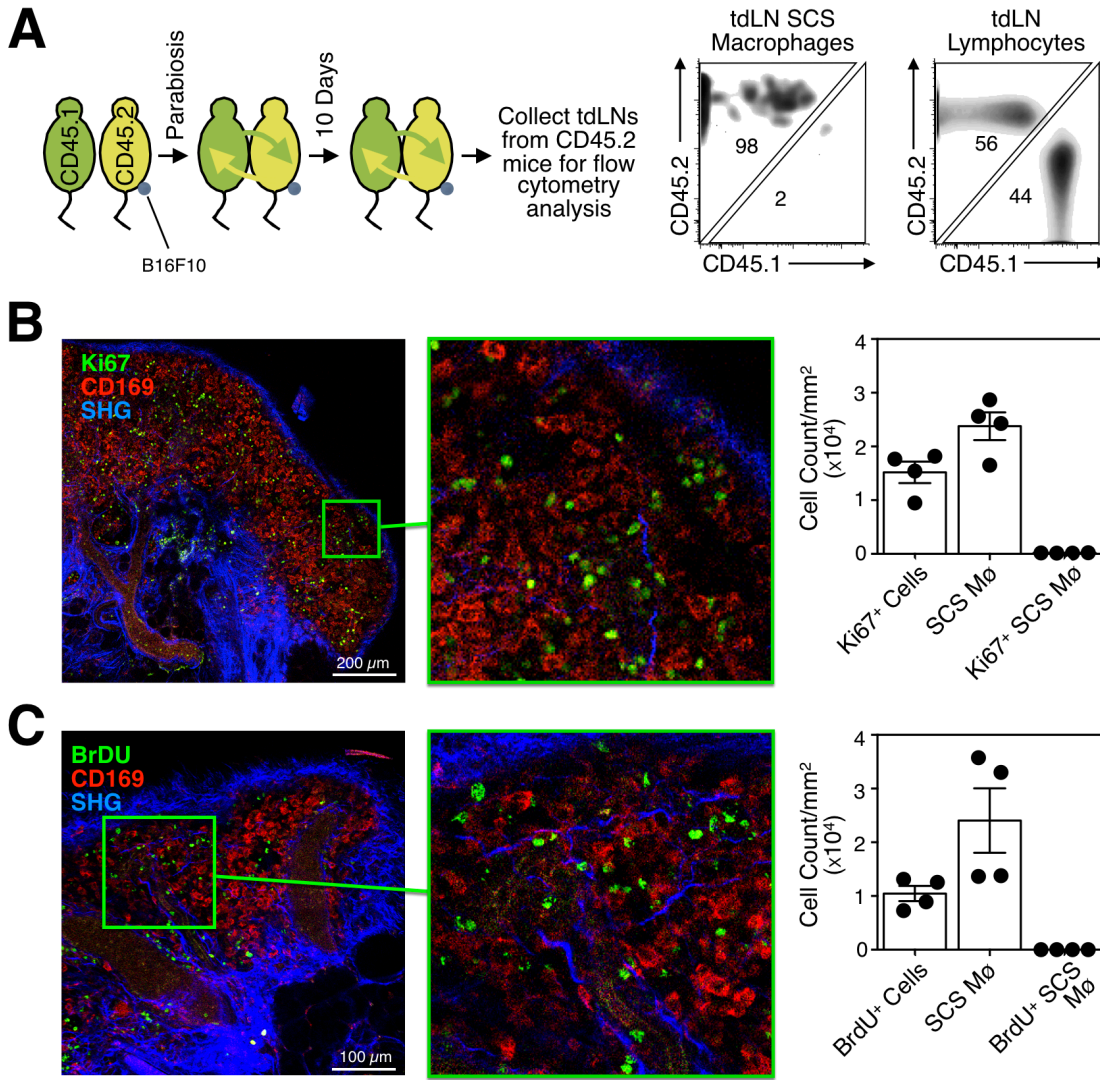


Fig. S21. SCS macrophages in tdLNs of B16F10 tumor-bearing mice neither are populated by circulating precursors nor proliferate locally. (A) Experimental outline of parabiosis study (left) and representative flow cytometry analysis of tdLN SCS macrophages (middle) and lymphocytes (right) collected from CD45.2 mice. (B) Representative multiphoton 2D reconstruction (left) and magnification (middle) of a tdLN stained for Ki67 (green) and CD169 (red). SHG is shown in blue. The number of green, red, and green+red cells per mm^2 is shown on the right ($n = 4$). (C) Representative multiphoton 2D reconstruction (left) and magnification (middle) of a tdLN stained for BrdU (green) and CD169 (red). BrdU was injected intraperitoneally 2 d before euthanasia. SHG is shown in blue. The number of green, red, and green+red cells per mm^2 is shown on the right ($n = 4$). BrdU = 5-bromo-2'-deoxyuridine; SCS = sub-capsular sinus; SHG = second harmonic generation; tdLN = tumor-draining lymph node. The parabiosis studies suggest that neither tumor-infiltrating cells nor circulating precursors contribute new SCS macrophages as tumors progress. Additionally, the BrdU and Ki67 labeling studies indicate that SCS macrophages do not detectably divide locally.

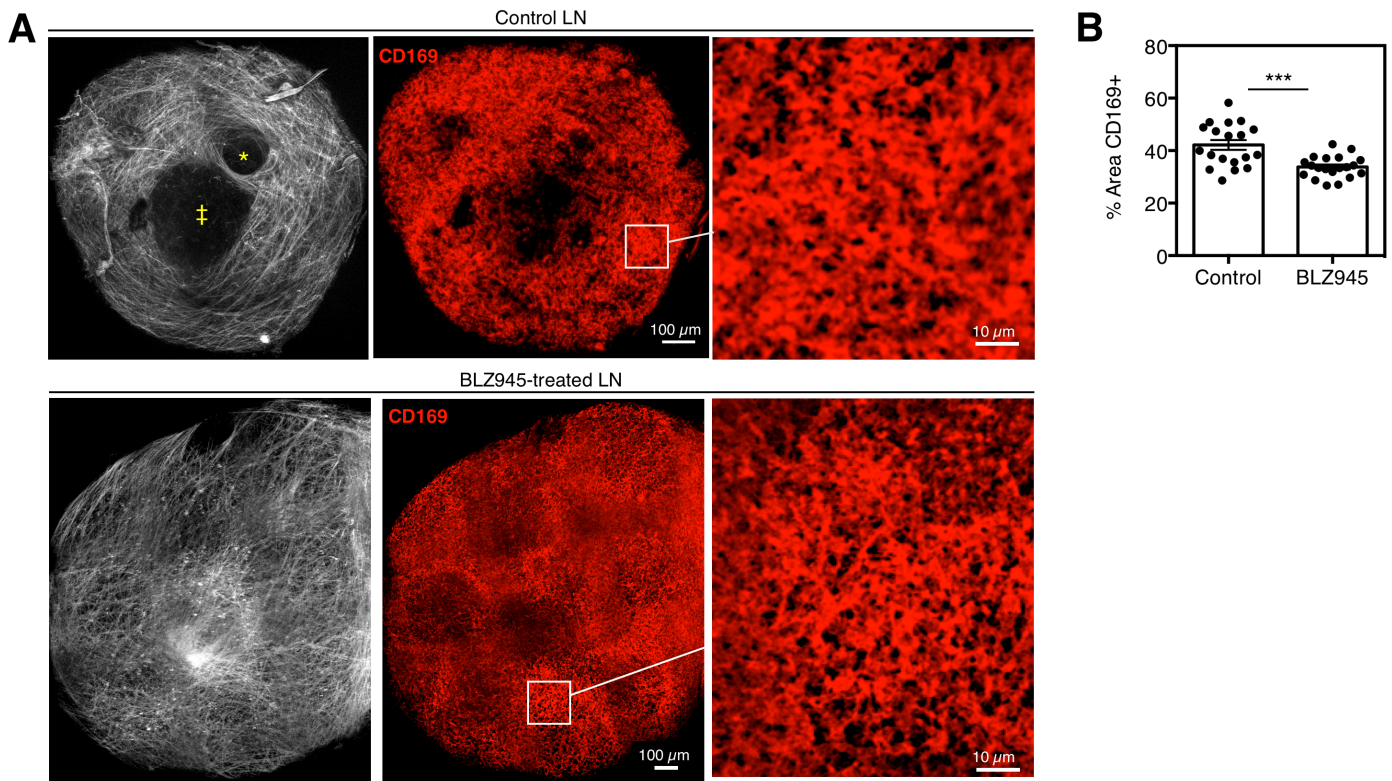


Fig. S22. Effect of CSF1-R inhibition on the SCS Mø barrier. (A) Multiphoton microscopy based quantification of SCS Mø barrier disruption (measured in B as % area covered by CD169⁺ SCS Mø) in LN after intraperitoneal injections of BLZ945 (5 daily injections). LNs are stained for CD169 (red). LN capsule (collagen visualized by second harmonic generation (SHG)) is in gray. Whole LN reconstructions were performed by combining optical section stitching and Z-axis projection. † = lymph vessel; ‡ = end of imaging volume. (n = 3). ***P < 0.001; Mann Whitney test.

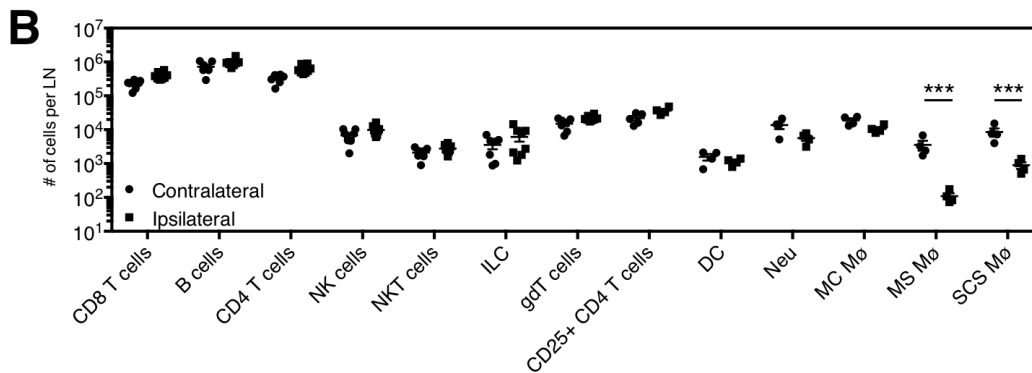
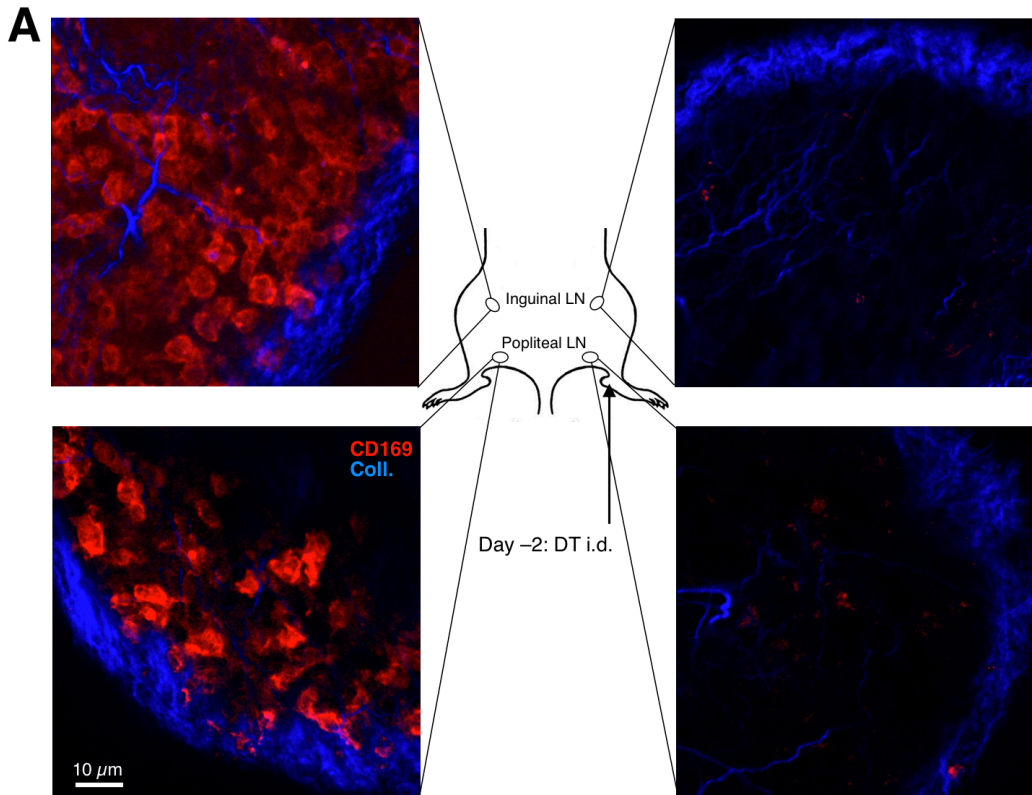


Fig. S23. Validation of local CD169⁺ SCS macrophage depletion with Diphtheria toxin (DT). (A) Multiphoton imaging of LNs from mice injected with low doses (250 ng) of DT locally (left calf). CD169 in red, LN capsule (Collagen) in blue (n = 2). (B) Flow cytometry based quantification of depletion specificity after DT administration (as in A) in Cd169^{Dtr/Wt} mice. Ipsilateral and contralateral inguinal LN are compared (n = 4-6). DC = dendritic cells; ILC = innate lymphoid cells; Mø = macrophages; MC = medullary cord; MS = medullary sinus; Neu = neutrophils; NK = natural killer; SCS = sub-capsular sinus. ***P < 0.001; Two-way ANOVA with Sidak's multiple comparisons test.

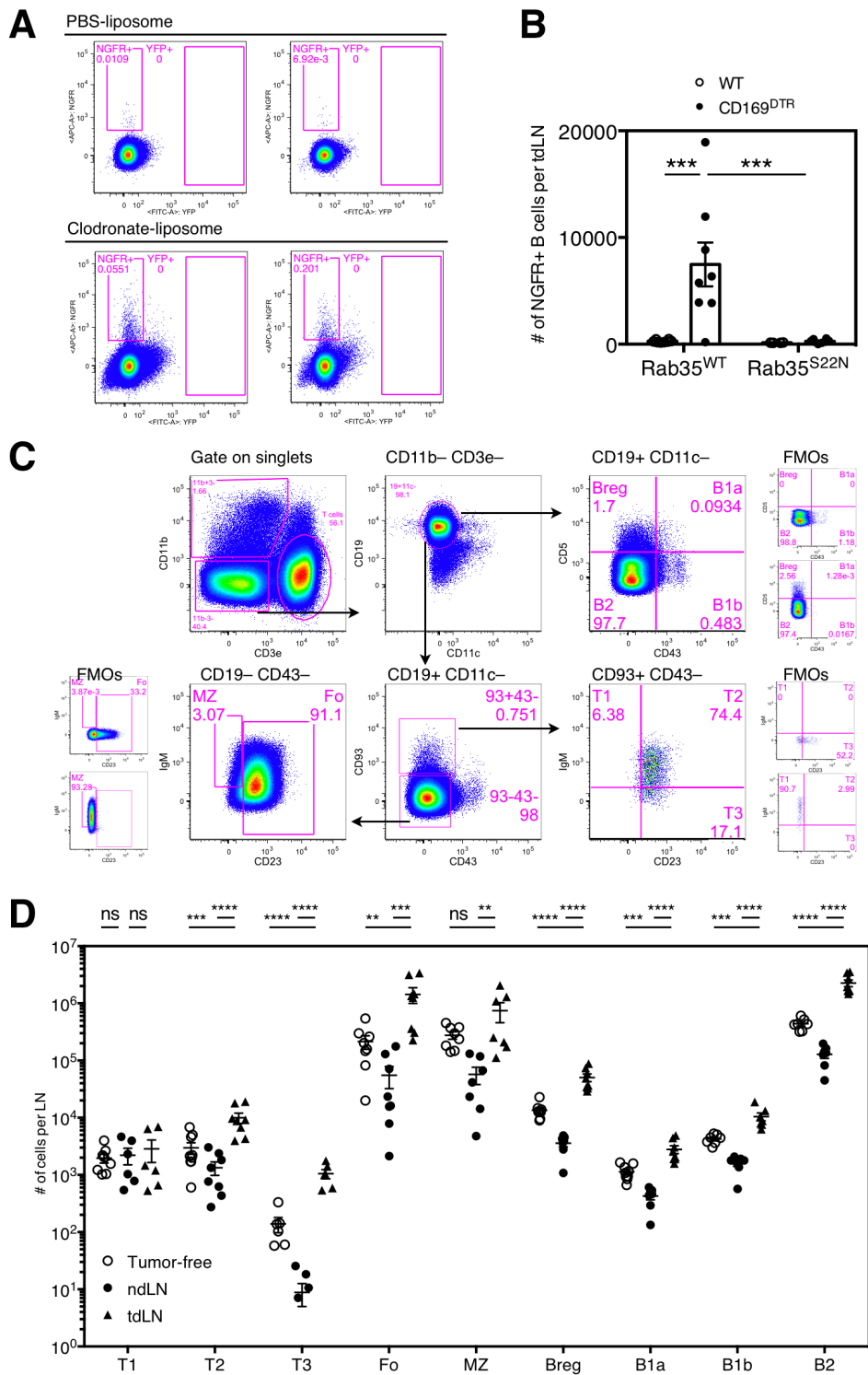


Fig. S24. Interaction of tEVs with B cells in tdLNs and B cell phenotypes in tdLNs and ndLNs. (A) Flow cytometry based analysis of tdLN B cells from Cre-reporter mice bearing dLNGFR⁺ CRE⁺ B16F10 tumors and that were treated with either PBS-liposomes (top panels) or clodronate-liposomes (bottom panels). Cre-reporter (YFP is shown on the X axis, tEV surface marker (dLNGFR) is shown on the Y axis. Two representative tdLNs from each group are shown (2 independent experiments; n = 6). (B) Flow cytometry based quantification of tEV⁺ B cells in tdLN from WT or Cd169^{Dtr/Wt} mice bearing Rab35^{WT} or Rab35^{S22N} expressing B16F10 melanomas (n = 5-8). (C) Gating strategy to study B cell subsets in LN. (D) Flow cytometry-based quantification of B cell subsets from naive LN, ndLN and tdLN (n = 6-8). tdLN = tumor-draining lymph node. **P < 0.01; ***P < 0.001; ****P < 0.0001; n.s.=not significant; Two-way ANOVA with Sidak's multiple comparisons test.

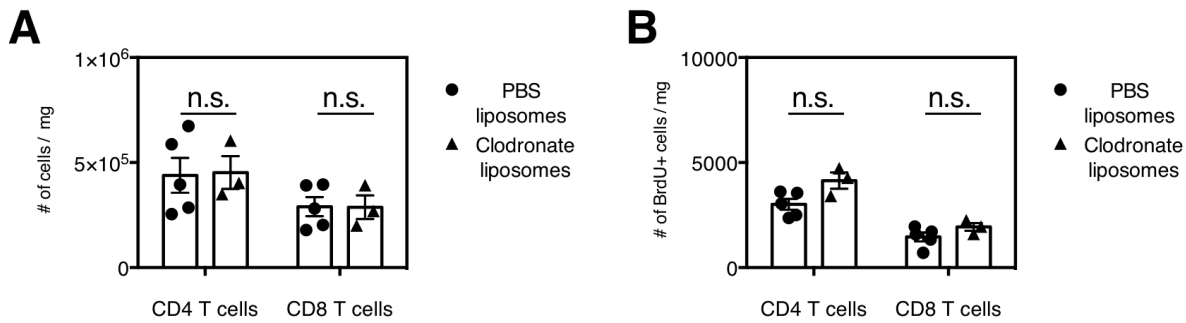


Fig. S25. T cell number and proliferation in tdLNs in presence or absence of CD169⁺ macrophages. (A-B) Flow cytometry based analysis of tdLN T cell subsets from B16F10 tumor-bearing mice (14 d after tumor challenge) that were treated with either PBS-liposomes or clodronate-liposomes. Total number of cells (**A**) and number of BrdU⁺ proliferating cells (**B**) per mg tissue are shown (n = 3-5). BrdU was injected intraperitoneally 2 d before euthanasia. tdLN = tumor-draining lymph node. n.s.=not significant; Two-way ANOVA with Sidak's multiple comparisons test. These results indicate that, although subcutaneously transferring dead tumor cells can elicit SCS macrophage-mediated T cell responses (38); both CD4⁺ and CD8⁺ T cells remained unchanged in tumors (Fig 4E) and tdLNs (this Supplemental Figure) of SCS macrophage-depleted mice.

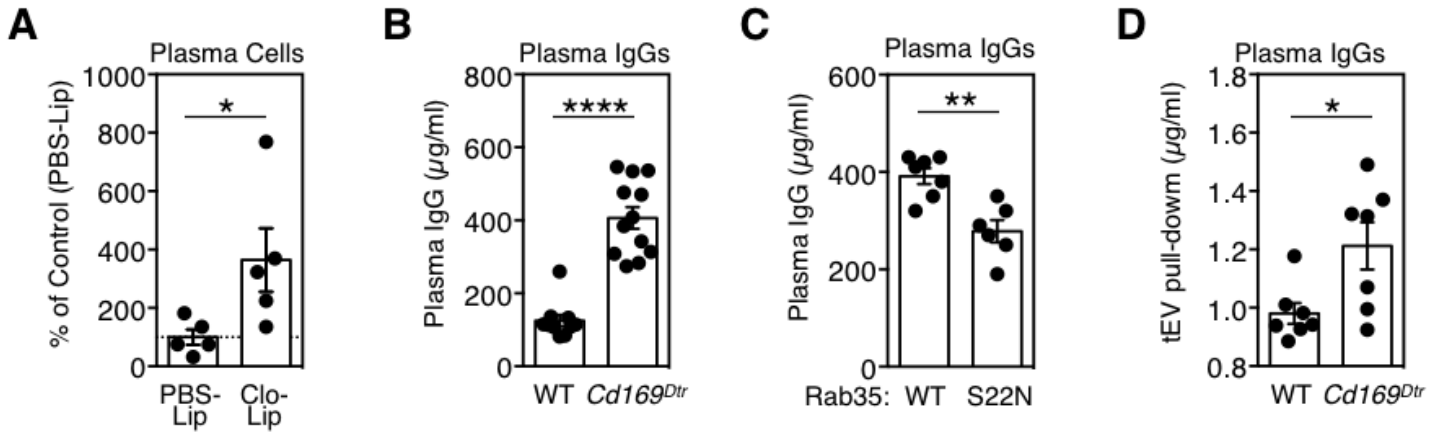
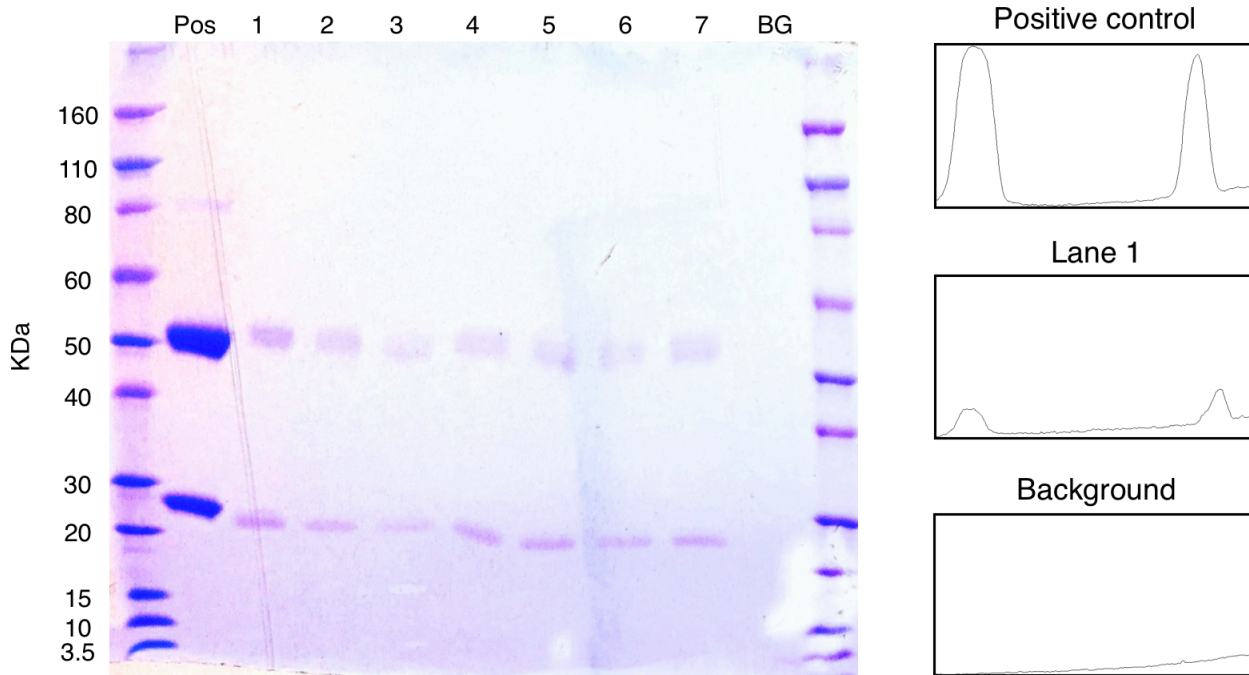


Fig. S26. IgG response in tumor-bearing mice depleted of CD169⁺ macrophages. (A) Flow cytometry-based quantification of plasma cells in tdLNs from B16F10 tumor-bearing mice treated with either PBS-liposomes (PBS-Lip) or clodronate liposomes (Clo-Lip) to deplete CD169⁺ LN macrophages (n = 5). (B) Plasma IgG quantification in WT and *Cd169^{Dtr/Wt}* mice treated with diphtheria toxin (2 independent experiments; n = 12). (C) Plasma IgG quantification in *Cd169^{Dtr/Wt}* mice treated with diphtheria toxin and challenged with Rab35^{WT} or Rab35^{S22N} expressing B16F10 melanomas (n = 6-7). (D) tEV pull-down with IgGs obtained from plasma of WT or *Cd169^{Dtr/Wt}* mice previously treated with diphtheria toxin (n = 7). The tEV pulldown experiment used Protein G columns loaded with IgGs from either control or DT-treated CD169^{Dtr/Wt} mice and then subjected to an equal quantity of PKH67 labeled tEVs. After washing, the IgGs were eluted off the column and tEV content measured by fluorescence (tEVs were detected by PKH67 labeling using a plate reader). *P < 0.05; **P < 0.01; ****P < 0.0001; Mann Whitney test. Taken together, these findings indicate that CD169⁺ macrophage depletion significantly amplified tdLN plasma cells and increased plasma IgG concentration. Such increase requires full-fledged tEV secretion by tumors because plasma IgG levels were lower in B16F10 Rab35^{S22N} tumor-bearing mice than in their B16F10 Rab35^{WT} counterparts. Also, IgGs from DT-treated mice pulled down a significantly greater amount of tEVs, suggesting that CD169⁺ macrophage-depleted mice are enriched with IgGs directed towards tEV antigens.



Suppl. Fig. 27. IgG preparations. To test the functional role of circulating IgGs in melanoma, we purified circulating IgGs from B16F10 tumor-bearing mice, in which SCS macrophages were either depleted or not, and injected those IgGs into SCS macrophage-competent, tumor-bearing mice. Here, the SDS gel shows IgGs isolated from tumor-bearing mice (left) and quantification of band intensities in representative lanes (right). Pos = positive control, commercial IgG; Background (BG) = no IgGs loaded.

Case No	Primary tumor (type, location)	Tumor depth	Ulceration	tdLN	LN metastasis	Detectable HMB45 ⁺ Mø
B2013.988	Superficial spreading melanoma, shoulder	0.65 mm	No	Axilla	No	Few*, 4/HPF
B2011.30185	Superficial spreading melanoma, back of hand	1.1 mm	No	Axilla	No	Few
B2013.38103	Superficial spreading melanoma, ear	1.26 mm	No	Parotis	No	Few, 4/HPF
B2011.7961	Superficial spreading melanoma, lower arm	1.3 mm	No	Axilla	No	Few, 1/HPF
B2010.38079	Superficial spreading melanoma, lower leg	1.6 mm	Yes	Inguinal	No	Few, 1/HPF
B2011.4216	Superficial spreading melanoma, shoulder	1.85 mm	Yes	Axilla	No	Few, 5/HPF
B2005.34421	Nodular melanoma, back	2 mm	Yes	Axilla	No	Few, 5/HPF
B2011.10923	Superficial spreading melanoma, elbow	2.4 mm	No	Axilla	No	None
B2014.10859	Acral melanoma	2.95 mm	No	Inguinal	No	Few, 8/HPF
B2013.9194	Nodular melanoma, shoulder	3.2 mm	No	Axilla	No	Moderate, 20/HPF
B2013.350	Head, parietal	>5 mm	Unknown	Cervical	No	Moderate, 8/HPF
B2014.13127	Nodular melanoma	7 mm	Yes	Axilla	No	Moderate, 15/HPF
B2014.17117	Animal type melanoma/atypical congenital nevus in a child, ear	Unknown	Unknown	Cervical	No	Numerous, >100/HPF
B2014.14441	Superficial spreading melanoma, lower arm	0.91 mm	No	Axilla	Yes	Moderate, 25/HPF

Table S1. Pathological characteristics of sentinel LNs and their primary tumors for each patient. Cancer-free sentinel LNs are tdLNs scored negative for metastases by pathologic evaluation. The table lists information for primary tumors (type, location, depth, ulceration) and sentinel LNs (location, presence of metastasis, detection of HMB-45⁺ macrophages) for each patient (case No) analyzed. HPF = high power field; LN = lymph node; Mø = macrophages. *Few: macrophages only visible at high power magnification; Moderate, macrophages readily visible at low magnification (100x); Numerous: macrophages present in every HPF with clusters containing up to 100 macrophages.

References

1. D. Hanahan, R. A. Weinberg, Hallmarks of cancer: The next generation. *Cell* **144**, 646–674 (2011). [Medline doi:10.1016/j.cell.2011.02.013](#)
2. S. S. McAllister, R. A. Weinberg, The tumour-induced systemic environment as a critical regulator of cancer progression and metastasis. *Nat. Cell Biol.* **16**, 717–727 (2014). [Medline doi:10.1038/ncb3015](#)
3. M. Colombo, G. Raposo, C. Théry, Biogenesis, secretion, and intercellular interactions of exosomes and other extracellular vesicles. *Annu. Rev. Cell Dev. Biol.* **30**, 255–289 (2014). [Medline doi:10.1146/annurev-cellbio-101512-122326](#)
4. H. Peinado, M. Alečković, S. Lavotshkin, I. Matei, B. Costa-Silva, G. Moreno-Bueno, M. Hergueta-Redondo, C. Williams, G. García-Santos, C. Ghajar, A. Nitadori-Hoshino, C. Hoffman, K. Badal, B. A. Garcia, M. K. Callahan, J. Yuan, V. R. Martins, J. Skog, R. N. Kaplan, M. S. Brady, J. D. Wolchok, P. B. Chapman, Y. Kang, J. Bromberg, D. Lyden, Melanoma exosomes educate bone marrow progenitor cells toward a pro-metastatic phenotype through MET. *Nat. Med.* **18**, 883–891 (2012). [Medline doi:10.1038/nm.2753](#)
5. J. Skog, T. Würdinger, S. van Rijn, D. H. Meijer, L. Gainche, M. Sena-Esteves, W. T. Curry Jr., B. S. Carter, A. M. Krichevsky, X. O. Breakefield, Glioblastoma microvesicles transport RNA and proteins that promote tumour growth and provide diagnostic biomarkers. *Nat. Cell Biol.* **10**, 1470–1476 (2008). [Medline doi:10.1038/ncb1800](#)
6. A. Zomer, C. Maynard, F. J. Verweij, A. Kamermans, R. Schäfer, E. Beerling, R. M. Schiffelers, E. de Wit, J. Berenguer, S. I. Ellenbroek, T. Würdinger, D. M. Pegtel, J. van Rheenen, In vivo imaging reveals extracellular vesicle-mediated phenocopying of metastatic behavior. *Cell* **161**, 1046–1057 (2015). [Medline doi:10.1016/j.cell.2015.04.042](#)
7. F. Pucci, M. J. Pittet, Molecular pathways: Tumor-derived microvesicles and their interactions with immune cells in vivo. *Clin. Cancer Res.* **19**, 2598–2604 (2013). [Medline](#)
8. S. A. Melo, L. B. Luecke, C. Kahlert, A. F. Fernandez, S. T. Gammon, J. Kaye, V. S. LeBleu, E. A. Mittendorf, J. Weitz, N. Rahbari, C. Reissfelder, C. Pilarsky, M. F. Fraga, D.

- Piwnicka-Worms, R. Kalluri, Glypican-1 identifies cancer exosomes and detects early pancreatic cancer. *Nature* **523**, 177–182 (2015). [Medline](#)
9. H. Shao, J. Chung, K. Lee, L. Balaj, C. Min, B. S. Carter, F. H. Hochberg, X. O. Breakefield, H. Lee, R. Weissleder, Chip-based analysis of exosomal mRNA mediating drug resistance in glioblastoma. *Nat. Commun.* **6**, 6999 (2015). [Medline](#)
[doi:10.1038/ncomms7999](https://doi.org/10.1038/ncomms7999)
10. C. P. Lai, O. Mardini, M. Ericsson, S. Prabhakar, C. A. Maguire, J. W. Chen, B. A. Tannous, X. O. Breakefield, Dynamic biodistribution of extracellular vesicles in vivo using a multimodal imaging reporter. *ACS Nano* **8**, 483–494 (2014). [Medline](#)
11. E. E. Gray, J. G. Cyster, Lymph node macrophages. *J. Innate Immun.* **4**, 424–436 (2012).
[Medline](#) [doi:10.1159/000337007](https://doi.org/10.1159/000337007)
12. A. M. Magnuson, G. M. Thurber, R. H. Kohler, R. Weissleder, D. Mathis, C. Benoist, Population dynamics of islet-infiltrating cells in autoimmune diabetes. *Proc. Natl. Acad. Sci. U.S.A.* **112**, 1511–1516 (2015). [Medline](#) [doi:10.1073/pnas.1423769112](https://doi.org/10.1073/pnas.1423769112)
13. H. Yaziji, A. M. Gown, Immunohistochemical markers of melanocytic tumors. *Int. J. Surg. Pathol.* **11**, 11–15 (2003). [Medline](#) [doi:10.1177/106689690301100103](https://doi.org/10.1177/106689690301100103)
14. H. Stenmark, Rab GTPases as coordinators of vesicle traffic. *Nat. Rev. Mol. Cell Biol.* **10**, 513–525 (2009). [doi:10.1038/nrm2728](https://doi.org/10.1038/nrm2728)
15. M. Gaya, A. Castello, B. Montaner, N. Rogers, C. Reis e Sousa, A. Bruckbauer, F. D. Batista, Inflammation-induced disruption of SCS macrophages impairs B cell responses to secondary infection. *Science* **347**, 667–672 (2015). [Medline](#)
[doi:10.1126/science.aaa1300](https://doi.org/10.1126/science.aaa1300)
16. V. Cortez-Retamozo, M. Etzrodt, A. Newton, P. J. Rauch, A. Chudnovskiy, C. Berger, R. J. Ryan, Y. Iwamoto, B. Marinelli, R. Gorbato, R. Forghani, T. I. Novobrantseva, V. Koteliensky, J. L. Figueiredo, J. W. Chen, D. G. Anderson, M. Nahrendorf, F. K. Swirski, R. Weissleder, M. J. Pittet, Origins of tumor-associated macrophages and neutrophils. *Proc. Natl. Acad. Sci. U.S.A.* **109**, 2491–2496 (2012). [Medline](#)
[doi:10.1073/pnas.1113744109](https://doi.org/10.1073/pnas.1113744109)

17. R. A. Franklin, W. Liao, A. Sarkar, M. V. Kim, M. R. Bivona, K. Liu, E. G. Pamer, M. O. Li, The cellular and molecular origin of tumor-associated macrophages. *Science* **344**, 921–925 (2014). [Medline doi:10.1126/science.1252510](#)
18. M. Iannacone, E. A. Moseman, E. Tonti, L. Bosurgi, T. Junt, S. E. Henrickson, S. P. Whelan, L. G. Guidotti, U. H. von Andrian, Subcapsular sinus macrophages prevent CNS invasion on peripheral infection with a neurotropic virus. *Nature* **465**, 1079–1083 (2010). [doi:10.1038/nature09118](#)
19. W. Kastenmüller, P. Torabi-Parizi, N. Subramanian, T. Lämmermann, R. N. Germain, A spatially-organized multicellular innate immune response in lymph nodes limits systemic pathogen spread. *Cell* **150**, 1235–1248 (2012). [Medline doi:10.1016/j.cell.2012.07.021](#)
20. E. A. Moseman, M. Iannacone, L. Bosurgi, E. Tonti, N. Chevrier, A. Tumanov, Y. X. Fu, N. Hacohen, U. H. von Andrian, B cell maintenance of subcapsular sinus macrophages protects against a fatal viral infection independent of adaptive immunity. *Immunity* **36**, 415–426 (2012). [Medline doi:10.1016/j.immuni.2012.01.013](#)
21. P. Andreu, M. Johansson, N. I. Affara, F. Pucci, T. Tan, S. Junankar, L. Korets, J. Lam, D. Tawfik, D. G. DeNardo, L. Naldini, K. E. de Visser, M. De Palma, L. M. Coussens, FcRγ activation regulates inflammation-associated squamous carcinogenesis. *Cancer Cell* **17**, 121–134 (2010). [Medline doi:10.1016/j.ccr.2009.12.019](#)
22. K. E. de Visser, L. V. Korets, L. M. Coussens, De novo carcinogenesis promoted by chronic inflammation is B lymphocyte dependent. *Cancer Cell* **7**, 411–423 (2005). [Medline doi:10.1016/j.ccr.2005.04.014](#)
23. P. M. Hogarth, G. A. Pietersz, Fc receptor-targeted therapies for the treatment of inflammation, cancer and beyond. *Nat. Rev. Drug Discov.* **11**, 311–331 (2012). [Medline doi:10.1038/nrd2909](#)
24. T. A. Wynn, A. Chawla, J. W. Pollard, Macrophage biology in development, homeostasis and disease. *Nature* **496**, 445–455 (2013). [Medline doi:10.1038/nature12034](#)
25. Y. R. Carrasco, F. D. Batista, B cells acquire particulate antigen in a macrophage-rich area at the boundary between the follicle and the subcapsular sinus of the lymph node. *Immunity* **27**, 160–171 (2007). [Medline doi:10.1016/j.immuni.2007.06.007](#)

26. T. Junt, E. A. Moseman, M. Iannacone, S. Massberg, P. A. Lang, M. Boes, K. Fink, S. E. Henrickson, D. M. Shayakhmetov, N. C. Di Paolo, N. van Rooijen, T. R. Mempel, S. P. Whelan, U. H. von Andrian, Subcapsular sinus macrophages in lymph nodes clear lymph-borne viruses and present them to antiviral B cells. *Nature* **450**, 110–114 (2007). [Medline doi:10.1038/nature06287](#)
27. T. G. Phan, J. A. Green, E. E. Gray, Y. Xu, J. G. Cyster, Immune complex relay by subcapsular sinus macrophages and noncognate B cells drives antibody affinity maturation. *Nat. Immunol.* **10**, 786–793 (2009). [Medline doi:10.1038/ni.1745](#)
28. C. H. Ries, S. Hoves, M. A. Cannarile, D. Rüttinger, CSF-1/CSF-1R targeting agents in clinical development for cancer therapy. *Curr. Opin. Pharmacol.* **23**, 45–51 (2015). [Medline doi:10.1016/j.coph.2015.05.008](#)
29. K. Ohnishi, Y. Komohara, Y. Saito, Y. Miyamoto, M. Watanabe, H. Baba, M. Takeya, CD169-positive macrophages in regional lymph nodes are associated with a favorable prognosis in patients with colorectal carcinoma. *Cancer Sci.* **104**, 1237–1244 (2013). [Medline doi:10.1111/cas.12212](#)
30. M. Amendola, M. A. Venneri, A. Biffi, E. Vigna, L. Naldini, Coordinate dual-gene transgenesis by lentiviral vectors carrying synthetic bidirectional promoters. *Nat. Biotechnol.* **23**, 108–116 (2005). [Medline doi:10.1038/nbt1049](#)
31. M. De Palma, L. Naldini, Transduction of a gene expression cassette using advanced generation lentiviral vectors. *Methods Enzymol.* **346**, 514–529 (2002). [Medline doi:10.1016/S0076-6879\(02\)46074-0](#)
32. M. DuPage, A. L. Dooley, T. Jacks, Conditional mouse lung cancer models using adenoviral or lentiviral delivery of Cre recombinase. *Nat. Protoc.* **4**, 1064–1072 (2009). [Medline doi:10.1038/nprot.2009.95](#)
33. S. Massberg, P. Schaerli, I. Knezevic-Maramica, M. Köllnberger, N. Tubo, E. A. Moseman, I. V. Huff, T. Junt, A. J. Wagers, I. B. Mazo, U. H. von Andrian, Immunosurveillance by hematopoietic progenitor cells trafficking through blood, lymph, and peripheral tissues. *Cell* **131**, 994–1008 (2007). [Medline doi:10.1016/j.cell.2007.09.047](#)

34. S. M. Pyonteck, L. Akkari, A. J. Schuhmacher, R. L. Bowman, L. Sevenich, D. F. Quail, O. C. Olson, M. L. Quick, J. T. Huse, V. Teijeiro, M. Setty, C. S. Leslie, Y. Oei, A. Pedraza, J. Zhang, C. W. Brennan, J. C. Sutton, E. C. Holland, D. Daniel, J. A. Joyce, CSF-1R inhibition alters macrophage polarization and blocks glioma progression. *Nat. Med.* **19**, 1264–1272 (2013). [Medline doi:10.1038/nm.3337](#)
35. F. Pucci, M. A. Venneri, D. Bizziato, A. Nonis, D. Moi, A. Sica, C. Di Serio, L. Naldini, M. De Palma, A distinguishing gene signature shared by tumor-infiltrating Tie2-expressing monocytes, blood “resident” monocytes, and embryonic macrophages suggests common functions and developmental relationships. *Blood* **114**, 901–914 (2009). [Medline doi:10.1182/blood-2009-01-200931](#)
36. E. E. Gray, S. Friend, K. Suzuki, T. G. Phan, J. G. Cyster, Subcapsular sinus macrophage fragmentation and CD169⁺ bleb acquisition by closely associated IL-17-committed innate-like lymphocytes. *PLOS ONE* **7**, e38258 (2012). [Medline doi:10.1371/journal.pone.0038258](#)
37. A. S. Payne, L. A. Cornelius, The role of chemokines in melanoma tumor growth and metastasis. *J. Invest. Dermatol.* **118**, 915–922 (2002). [Medline doi:10.1046/j.1523-1747.2002.01725.x](#)
38. K. Asano, A. Nabeyama, Y. Miyake, C. H. Qiu, A. Kurita, M. Tomura, O. Kanagawa, S. Fujii, M. Tanaka, CD169-positive macrophages dominate antitumor immunity by crosspresenting dead cell-associated antigens. *Immunity* **34**, 85–95 (2011). [Medline doi:10.1016/j.immuni.2010.12.011](#)